Pathways towards True Catalysts: Computational Modelling and Structural Transformations of Zn-Polyoxotungstates

Supporting Information

Lubin Ni, Robin Güttinger, C. A. Triana, Bernhard Spingler,
Kim K. Baldridge, and Greta R. Patzke**

Table of Contents

III. Analytical characterization of the Zn/Sb-POM family

IV. Computational modelling of the reaction process

V. Catalytic performance of the Zn/Sb-POM family

VI. Analytical characterization of the true catalyst

Experimental Section

Materials and analytical characterizations. $Na_9[B\text{-}\alpha\text{-}SbW_9O_{33}]\cdot19.5H_2O$ as precursor material was prepared according to literature protocols[S1] and its purity was confirmed by FT-IR spectroscopy. Other chemicals were commercially purchased and used without further purification. Elemental analyses of all polyanions were performed by Mikroanalytisches Labor Pascher, Remagen, Germany. Fourier transform infrared (FT-IR) spectra were recorded on a Bruker Optics Vertex 70 Spectrometer. Raman spectroscopy was performed on a Renishaw Ramascope 1000 with a green SpectraPhysics Argon laser with a wavelength of 524.5 nm and 50 mW capacity. TG measurements were conducted on a Netzsch STA 449 C between 25 and 800 °C with a heating rate of 5 K min^{-1} in nitrogen atmosphere. UV/vis spectra were recorded on a Perkin-Elmer Lambda 650S spectrometer. Cyclic voltammetry experiments were performed on a Metrohm Computrace Voltammetric Analyzer model 757 VA. The system was operated with 757 VA Computrace software (Metrohm). The three-electrode cell system consisted of a 2 mm glassy carbon working electrode (GCE, modified or unmodified), a saturated Ag/AgCl reference electrode and a Pt wire as the counter electrode.

Synthesis of $Na_9Zn[Zn_4Na_2(H_2O)_8(SbW_9O_{33})_2][Zn_{2.6}Na_{0.4}(H_2O)_{2.6}(SbW_9O_{33})_2]\cdot45H_2O$ **{Zn_4-$Zn_{5.2}$ (1a)}**. 0.754 g (0.26 mmol) of $Na_9[SbW_9O_{33}]\cdot19.5H_2O$ was dissolved in 25 mL of water and heated to 85 ºC under stirring. After 20 min, 0.259 g (0.90 mmol) of $Zn(SO_4)_2\cdot7H_2O$ was added in individual portions at pH values around 5.5 ~ 6.5. The solution was left stirring for 90 min at 85 ºC, cooled to room temperature and filtered. Slow evaporation of the solution afforded colorless crystals. Yield: 0.468 g, 62.3% based on W. TGA showed a weight loss of 10.5% in the 30 - 240 °C temperature range, corresponding to the loss of coordinating and solvent water molecules (expected 11.2%). FT-IR (cm^{-1}): 1624(vs), 1140(m), 1119(m), 946(vs), 897(vs), 834(s), 728(m), 634(m), 519(m), 470(w). Raman (cm^{-1}): 961(vs), 888(s), 848(m), 797(w), 695(w), 515(w), 312(m), 224(m). Elemental analysis calcd. (found). W 57.29 (57.90); Zn 6.03 (6.24); Sb 4.21 (4.29); Na 2.92 (3.44); H 1.27 (1.12).

Synthesis of
$NaZnH_8[Zn_4Na_2(H_2O)_8(SbW_9O_{33})_2][Zn_{2.6}Na_{0.4}(H_2O)_{2.6}(SbW_9O_{33})_2]\cdot46H_2O$ **{Zn_4-$Zn_{5.2}$ (1b)}**.

The synthesis was performed as described above for **Zn_4-$Zn_{5.2}$ (1a)** with one alteration: 5~8 drops NH_4Cl solution (1.0 M) were added dropwise to the filtrate. Slow evaporation of the solution can afford colorless crystals **Zn_4-$Zn_{5.2}$ (1a)** mixed with small amounts of other block-shaped crystals of **Zn_4-$Zn_{5.2}$ (1b)**. FT-IR (cm^{-1}): 1629(vs), 939(vs), 838(vs), 675(m), 621(m), 514(m), 432(w). Raman (cm^{-1}): 966(vs), 885(s), 848(m), 700(w), 530(w), 448(w), 373(m), 318(m), 225(m). Elemental analysis calcd. (found). W 58.17 (56.90); Zn 6.13 (5.84); Sb 4.28 (4.27); Na 0.81 (3.00); H 1.34 (1.16).

Synthesis of $Na_8(NH_4)_2H_9\{[Zn_5NaCl_3(H_2O)_4(SbW_9O_{33})_2][Zn_{5.2}Na_{0.8}(H_2O)_{5.2}(SbW_9O_{33})_2]\}[SbCl_6]_{0.5}\cdot 43H_2O$ **{Zn$_5$-Zn$_{5.2}$ (2)}**, $Na_4H_9[Zn_6(H_2O)Cl_5(SbW_9O_{33})_2]\cdot 44H_2O$ **{Zn$_6$ (3a)}**, and $Na_2H_7[Zn_5Na(H_2O)_5Cl_2(SbW_9O_{33})_2]\cdot 33H_2O$ **{Zn$_5$ (4)}**.

The above synthetic procedure was modified by the addition of 10~20 drops NH_4Cl solution (1.0 M) to the filtrate. Slow concentration at room temperature led to the formation of large block-shaped crystals of $Na_2Zn(SO_4)_2\cdot 4H_2O$ as a side product together with a mixture of **{Zn$_5$-Zn$_{5.2}$ (2)}**, **{Zn6 (3a)}** and **{Zn$_5$ (4)}**. As the narrow preparative window for these compounds renders their separation practically impossible, we summarize their crystallographic data in Table S1.

Synthesis of $(NH_4)_{12}[Zn_6Cl_6(SbW_9O_{33})_2]\cdot 16H_2O$ **{Zn$_6$ (3b)}**. The synthetic method for **Zn$_6$ (3b)** is similar as described above for the synthesis of **Zn$_4$-Zn$_{5.2}$ (1a)** except for addition of 30~80 drops NH_4Cl solution (1.0 M) to the filtrate. Slow evaporation of the solution afforded colorless crystals. Yield: 0.391g, 53.3% based on W. TGA showed a weight loss of 5.0% in the 30-198 °C temperature range, corresponding to the loss of coordinating and solvent water molecules (expected 5.0%), followed by a slower weight loss of 7.9% between 202 – 515 °C caused by release of ammonia and hydrogen chloride (expected 7.6%). FT-IR (cm^{-1}): 1618(vs), 1408(vs), 970(m), 946(vs), 894(vs), 858(s), 826(s), 708(m), 665(m), 522(m), 470(w). Raman (cm^{-1}): 968(vs), 936(m), 886(w), 843(s), 693(w), 522(w), 312(m), 223(m). Elemental analysis calcd. (found): W 57.87 (58.30); Zn 6.86 (6.77); Sb 4.26 (4.30); Cl 3.72 (3.39); N 2.93 (2.13); H 1.41 (1.10).

Synthesis of $Na_7[Zn_5Na(H_2O)_5(CH_3COO)_2(SbW_9O_{33})_2]\cdot 27H_2O$ **{Zn$_5$(5a)}** and $Na_6H_4[Zn_5Na(H_2O)_4Cl(CH_3COO)_2(SbW_9O_{33})_2]\cdot 36H_2O$ **{Zn$_5$(5b)}**.

Method for **Zn$_5$ (5a)**: 0.190 g (0.87 mmol) of $Zn(OAc)_2\cdot 2H_2O$ was dissolved in 25 mL of water and heated to 85 °C under stirring. After 20 min, 0.754 g (0.26 mmol) of $Na_9[SbW_9O_{33}]\cdot 19.5H_2O$ was added in individual portions at pH values around 6.0 ~ 6.5. The mixture was left stirring for 90 min at 85 °C, cooled to room temperature and filtered. Slow evaporation of the solution afforded colorless crystals (**5a**; yield: 0.294 g, 38.8% based on W. TGA showed a weight loss of 9.9% in the 30 - 190 °C range, corresponding to the loss of coordinating and solvent water molecules (expected 10.2%), followed by a slower weight loss of 2.0% between 200 – 408 °C caused by release of acetate ligands (expected 2.6%). FT-IR (cm^{-1}): 1622(vs), 1411(s), 929(vs), 870(vs), 846(s), 698(vs), 626(s), 503(m), 430(w).
Raman (cm^{-1}): 959(vs), 932(m), 893(s), 846(m), 695(w), 514(w), 314(m), 223(m). Elemental analysis calcd. (found): W 56.90 (55.40); Zn 5.62 (5.51); Sb 4.18 (4.10); Na 3.16 (3.55); C 0.82 (0.66); H 1.23 (0.87).

For **Zn$_5$ (5b)**: 0.754 g (0.26 mmol) of $Na_9[SbW_9O_{33}]\cdot 19.5H_2O$ was dissolved in 25 mL of water and heated to 85 °C under stirring. After 20 min, 0.300 g (1.37 mmol) of $Zn(OAc)_2\cdot 2H_2O$ was added in individual portions. The solution underwent a color change to light yellow at pH values around 6.0 ~ 6.5.

The mixture was left stirring for 90 min at 85 °C, cooled to room temperature and filtered. Addition of 5 drops NH_4Cl solution (1.0 M) to the yellow filtrate, followed by slow evaporation of the solution afforded colorless crystals **(5b)** mixed with small amount of yellow crystal of $Na_{14}[\beta\text{-}Zn_2Sb^{III}_2(ZnW_9O_{34})_2].46H_2O$.[S 2] TGA showed a weight loss of 9.6% in the 30 – 210 °C range, corresponding to the loss of coordinating and solvent water molecules (expected 11.0%), followed by a slower weight loss of 3.6% between 210 – 446 °C caused by release of acetate ligands and hydrogen chloride (expected 2.6%). FT-IR (cm^{-1}): 1622(vs), 1411(s), 929(vs), 870(vs), 846(s), 698(vs), 626(s), 503(m), 430(w). Raman (cm^{-1}): 960(vs), 934(m), 892(s), 843(m), 783(w), 688(w), 514(w), 444(w), 314(m), 223(m). Elemental analysis calcd. (found): W 55.51 (55.90); Zn 5.48 (5.32); Sb 4.08 (4.22); Na 3.08 (3.11); Cl 0.59 (0.48); C 0.80 (0.67); H 1.44(1.29).

Synthesis of $Na_5H_4[Zn_4Na_2(H_2O)_7(CH_3COO)(SbW_9O_{33})_2]\cdot 28H_2O$ **{Zn$_4$(6a)}** and $Na_5(NH_4)_5H_2[Zn_{4.1}Na_{1.9}Cl_3(H_2O)_7(CH_3COO)(SbW_9O_{33})_2]\cdot 24.5H_2O$ **{Zn$_4$ (6b)}**.

The synthetic method for **Zn$_4$(6a)** is similar as described above for the synthesis of **Zn$_5$(5a)** with one alteration: addition of 5-10 drops NH_4Cl solution (1.0 M) to the filtrate. Slow evaporation of the solution afforded colorless crystals. Yield: 0.545 g, 73% based on W. TGA showed a weight loss of 7.8% in the 30-160 °C range, corresponding to the loss of coordinating and solvent water molecules (expected 7.9 %). FT-IR (cm^{-1}): 1628(s), 1571(s), 1413(s), 937(vs), 888(vs), 848(s), 712(m). 679(m), 503(m), 430(w). Raman (cm^{-1}): 959(vs), 875(s), 848(s), 799(w), 690(w), 517(w), 316(m), 225(m). Elemental analysis calcd. (found): W 58.10 (57.00); Zn 4.59 (4.69); Sb 4.28 (4.21); Na 3.23 (3.53); N 0.73 (0.51); H 1.29(1.12), C 0.42 (0.68).

The method for **Zn$_4$(6b)** is similar as described above for the synthesis of **Zn$_5$(5a)** except for the addition of 30-40 drops NH_4Cl solution (1.0 M) to the filtrate. Slow evaporation of the solution afforded colorless crystals. Yield: 0.308 g, 40% based on W. TGA showed a weight loss of 8.9% in the 30 – 205 °C range, corresponding to the loss of coordinating and solvent water molecules (expected 8.5%), FT-IR (cm^{-1}): 1626(s), 1414(s), 931(vs), 871(vs), 848(vs), 702(s), 684(s), 625(m), 503(m), 430(w). Raman (cm^{-1}): 1041(m), 968(vs), 935(s), 898(s), 851(s), 782(w), 693(w), 517(w), 449(w), 319(m), 223(m). Elemental analysis calcd. (found): W 56.63 (57.10); Zn 4.47 (4.65); Sb 4.16 (4.23); Na 2.36 (2.94); Cl 1.82 (0.59); N 1.19 (1.34); H 1.55(1.46), C 0.41 (0.45).

Synthesis of $(NH_4)_4Na_7[Zn_4Na_2Cl_3(H_2O)_5(SbW_9O_{33})_2]\cdot 16H_2O$ **{Zn$_4$ (6c)}** and $Na_{6.5}H_4[Zn_{3.5}Na_{2.5}Cl_2(H_2O)_{6.5}(SbW_9O_{33})_2]\cdot 25H_2O$ **{Zn$_{3.5}$ (7)}**.

The method is similar as described above for the synthesis of **Zn$_5$ (5a)**. The only alteration is the addition of 15-25 drops of NH_4Cl solution (1.0 M) to the filtrate. Slow evaporation of the solution afforded a mixture of three crystal types (**6a**, **6c**, and **7**).

For **Zn_4 (6c)**: TGA showed a weight loss of 7.3% in the 30 - 180 °C range, corresponding to the loss of coordinating and solvent water molecules (expected 6.7%), followed by a slower weight loss of 2.9% between 180 – 410 °C caused by release of ammonia and hydrogen chloride (expected 3.2%). FT-IR (cm^{-1}): 1626(s), 1404(s), 935(vs), 876(s), 837(s), 716(m), 673(m), 509(m), 431(w). Raman (cm^{-1}): 966(vs), 890(s), 878(s), 791(w), 697(w), 529(w), 324(m), 229(m). Elemental analysis calcd. (found): W 58.73 (56.40); Zn 4.64 (4.81); Sb 4.32 (4.81); Cl 1.88 (1.58); H 1.03 (1.28); N 0.99 (1.00).

For **$Zn_{3.5}$ (7)**: TGA showed a weight loss of 9.6% in the 30 - 210 °C range, corresponding to the loss of coordinating and solvent water molecules (expected 10.0 %). FT-IR (cm^{-1}): 1628(s), 1419(s), 928(vs), 867(vs), 851(s), 698(m), 500(m), 431(w). Raman (cm^{-1}): 953(vs), 895(s), 878(s), 794(w), 687(w), 518(w), 442(w), 318(m), 231(m). Elemental analysis calcd. (found): W 58.53 (56.50); Zn 4.04 (4.29); Sb 4.31 (4.21); Cl 1.25 (0.97); H 0.60 (1.00).

Synthesis of $Na_9[Zn_3Na_3(H_2O)_9(SbW_9O_{33})_2]\cdot 42H_2O$ **{Zn_3 (8)}**

The polyanion $[Zn_3(H_2O)_3(SbW_9O_{33})_2]^{12-}$ has been first reported by *Kortz* et al in 2001.[S3] We here explored a different synthetic route to this compound. The method for **Zn_3(8)** was similar as described above for the synthesis of **Zn_4-$Zn_{5.2}$(1a)** with one alteration: 0.863 g (3 mmol) $Zn(SO_4)_2\cdot 7H_2O$ was used instead of 0.259 g (0.90 mmol). Yield: 0.523g, 67.5 % based on W.

Synthesis of $Na_7Cs_2Zn_{1.6}H_{1.8}[Zn_2(H_2O)_6(WO)_2(\beta\text{-}SbW_9O_{33})_2]Cl_4\cdot 32H_2O$ **{Zn_2W_2} (9)**.

The polyanion $[Zn_2(H_2O)_6(WO_2)_2(\beta\text{-}SbW_9O_{33})_2]^{10-}$ has been first reported by *Krebs* et al in 2002.[S4] We here explored a different route to the Cs^+ salt of $[Zn_2Sb_2W_{20}O_{70}]^{10-}$ **(9)**: 0.754 g (0.26 mmol) of $Na_9[SbW_9O_{33}]\cdot 19.5H_2O$ was dissolved in 25 mL of sodium acetate buffer (0.5 M, pH 4.4) and heated to 85 °C under stirring. After 20 min, 0.259 g (0.90 mmol) of $Zn(SO_4)_2\cdot 7H_2O$ and 0.659 g (2.00 mmol) $Na_2WO_4\cdot 2H_2O$ were added in individual portions. The solution was left stirring for 90 min at 85 °C, cooled to room temperature and filtered. Addition of 1.0 M CsCl solution (0.5 mL) to the colorless filtrate and slow evaporation at room temperature afforded colorless crystals.

Catalytic alcohol oxidation. Oxidation reactions were carried out in a 10 mL round-bottom flask. Catalyst, solvent, substrate, and 30% aqueous H_2O_2 were successively placed into the round-bottom flask. A Teflon-coated magnetic stirring bar was added and the reaction mixture was stirred at 85 °C. Detailed reaction conditions are given in the caption of Table 1. All yields reported in this manuscript are based on alcohol conversion. Reaction products were characterized and quantified with a gas chromatograph (Finnigan Trace GC Ultra) equipped with a flame ionization detector and fitted with a ZB-5MS Phenomenex column (30 m length, 0.25 mm internal diameter, 0.25 μm film thickness) using dodecane as internal reference. Products were furthermore identified by GC-MS (Finnigan Trace DSQ GC-MS systems).

X-ray crystallography. Data collection of all compounds was performed on an Oxford Xcalibur Ruby CCD single-crystal diffractometer (MoK$_\alpha$ radiation, λ= 0.71073 Å) at 183(2) K. Routine Lorentz and polarization corrections were applied, and an absorption correction was performed using the program *CrysAlis* (multi-scan).[S 5] Structural analyses were performed using the *Win-GX for Windows* software.[S6] Direct methods were used to locate heavy metal atoms (SHELXS-97). The remaining atoms were located from successive Fourier maps (SHELXL-97).[S7] Further details on the crystal structure data can be obtained from ICSD/FIZ Karlsruhe via www.fiz-karlsruhe.de/icsd.html (fax (+49) 7247-808-666; e-mail crysdata@fiz-karlsruhe.de), on quoting the depository numbers CSD 426348-426359 for all compounds. Hydrogen atoms were not included in the refinements. Heavy metal atoms (Sb, Zn, W and Na) were refined anisotropically, and oxygen atoms were refined isotropically. The lighter atoms in POMs are generally difficult to refine anisotropically due to the presence of manifold heavy metal atoms.[S8] The Zn7 and Na3 sites are site-occupancy disordered with the occupancies of 0.6 (0.4) for Zn7 (Na3) in **(1a)**. For **(1b)**, W6 and W7 exhibit a disorder over two positions with site occupancies of 0.7 and 0.3 respectively. W10, W15, W16, W17, W18, W23, W24 and W31 are site-occupancy disordered with half occupancies each. Zn6 and Na2 are site-occupancy disordered with occupancies of 0.6 for Zn6 and 0.4 Na2 in **(2)**. O33 and Cl2 sites attached to the Zn2 atom are site-occupancy disordered with quarter occupancies in **(3a)**; as Cl2 is located on the mirror plane, this result in one half-occupied chloride and two quarter occupied water molecules adjacent to the mirror plane. Zn3 and Na1 sites are site-occupancy disordered with half occupancies each in **(4)**. Na1 and Zn5 sites are site-occupancy disordered with occupancies of 0.9 for Na1 and 0.1 for Zn5 in **(6b)**, Finally, Zn2 and Na3 sites are site-occupancy disordered with half occupancies each in **(7)**.

X-ray absorption spectroscopy. XAS experiments at the W-L_3 and Zn-K edges on solid samples dispersed in cellulose of pristine and post-catalytic $[Zn_6Cl_6(SbW_9O_{33})_2]^{12-}$, and reference compounds $[WZn_3(H_2O)_2(ZnW_9O_{34})_2]^{12-}$, $[SbW_9O_{33}]^{12-}$ and $Na_2WO_4{\cdot}2H_2O$ were carried out at the SuperXAS beamline Swiss Light Source (SLS) at the Paul Scherrer Institut, Villigen, Switzerland. The storage ring was run in top-up mode with an average current of 400 mA. The X-ray beam was collimated using a Si coated mirror and the energy was scanned using a channel-cut Si[111] monochromator. Energy calibration was done using a metal W foil. A toroidal mirror with Rh coating was used after the monochromator to focus the incident X-rays with a spot size of 140×120 μm^2 on the samples (photon flux of 3.3×10^{11} photons/s). Measurements were done in transmission mode using a 5-element Silicon Drift Detector. The measured EXAFS spectra $k^3\chi(k)$ were extracted by standard data reduction, absorption edge energy calibration and background subtraction as implemented in ATHENA. [S9] The spectra were reduced in the range $\Delta k\approx3$-12 Å^{-1} and Fourier-Transformed to FT$|k^3\chi(k)|$ in the real-space interval ΔR$\approx$0-6 Å. To calculate main values for interatomic distances, coordination numbers (N), and Debye-Waller factors (σ^2), nonlinear least-squares fitting of the FT$|k^3\chi(k)|$ spectra was done by ARTEMIS[S 9] using atomic clusters of $[Zn_6Cl_6(SbW_9O_{33})_2]^{12-}$, $[WZn_3(H_2O)_2(ZnW_9O_{34})_2]^{12-}$ (CCDC:

1628204), $[SbW_9O_{33}]^{12-}$ (ICSD: 406489) and $Na_2WO_4·2H_2O$ (ICSD: 240882) generated by ATOMS[S9] as implemented in IFEFFIT.[S9] Amplitudes and phase shifts for single and multiple scattering paths were calculated using the FEFF6 code.[S10]

Computational Details. Computed structure and property results were carried out using the GAMESS[S11] Gaussian09[S12] software packages. The conformational analyses of the molecular systems described in this study, including structural and orbital arrangements as well as property calculations, were carried out using the BP86 density functional level of theory[S13], [S14] in combination with a) the effective core potential/basis set combination, LANL2DZ+f,[S15] and b) Def2-TZVPP basis set.[S16] The LANL2DZ basis set is of double-ζ quality in the valence and "valence-1" shells, while the RECP contains Darwin and mass-velocity contributions; inclusion of f basis functionality was included.[S17], [S 18], [S 19] The Def2-TZVPP basis set is a all electron triple-ζ quality basis set. Full geometry optimizations were performed and uniquely characterized via second derivatives (Hessian) analysis to determine the number of imaginary frequencies (0=minima; 1=transition state), and effects of zero point energy. Effects of solvation were taken into account using the COSab method,[S20],[S21] using a dielectric for water and solvent radii from Klamt.[S22] Visualization and analysis of structural and property results were obtained using Avogadro[S23] and WEBMO.[S24]

Reverse Monte Carlo (RMC). To simulate the disordered structure of the true catalyst emerging from $[Zn_6Cl_6(SbW_9O_{33})_2]^{12-}$ the W-L_3 and Zn-K edge EXAFS spectra FT$|k^3\chi(k)|$ [Δr≈0-6 Å] was fitted by RMC simulations as implemented in RMCProfile.[S25] The atoms were constrained to move into cutoff distances W-O≈1.6-2.3 Å, W-W≈3.1-3.8 Å, Zn-O≈1.8-2.8 Å, Zn-Zn≈3.0-3.3 Å and Zn-W≈3.2-3.8 Å. To preserve the bonding the stretching potentials W-O 0.984 eV (1.99 Å) and Zn-O 0.984 eV (2.2 Å) were used, and their weightings were optimized at each RMC run. RMC-EXAFS fitting was implemented by allowing 1-3% of atoms to undergo displacements of ≈0.01-0.03 Å at each RMC run. Total FT$|k^3\chi(k)|$ spectra equal to the averaged single spectrum of each photoabsorbing W and Zn atoms were re-calculated at each RMC run. Each atomic movement was tested according to the consistency R^2 degree between the experimental and refined spectral-data-points as described in detailed references.[S26]

II. Structural characterization of the Zn/Sb-POM family

Single-crystal X-ray diffraction shows that **Zn_6(3b)** consists of two $[B\text{-}\alpha\text{-}SbW_9O_{33}]^{9-}$ units connected by a hexagonal Zn_6 ring $[Zn_6Cl_6O_{12}]$ with D_{3d} symmetry (Figure 1a). Each of the zinc atoms displays a related five-fold coordinated $[ZnO_4Cl]$ environment with square-pyramidal geometry, consisting of four terminal oxygen atoms from two **{SbW_9}** units with Zn-O bond lengths of 2.061(8) – 2.077(8) Å and one chlorine atom Zn-Cl, with bond length of 2.222(1) Å (Figure 1b). Six zinc atoms form an approximately equatorial hexagon by sharing their oxygen atoms (Figure 1b). The remaining members of the $\{Zn_nNa_{6-n}(B\text{-}\alpha\text{-}SbW_9O_{33})_2\}$ (n = 3-6) series either display complete Zn cores, such as in **Zn_6(3b)**, or partial substitution of Zn by Na atoms (cf. Figure 1c and Supporting Information for a detailed description of the individual compounds).

For example, two independent sandwich-type polyoxoanions coexist in the asymmetric units of **{Zn_4_$Zn_{5.2}$}(1a, 1b)** or **{Zn_5_$Zn_{5.2}$}(2)**, respectively (Figure 1c). Both compounds **(1a** and **1b)** contain the same polyanions of $[Zn_4Na_2(H_2O)_8(SbW_9O_{33})_2]^{8-}$ together with $[Zn_{5.2}Na_{0.8}(H_2O)_{5.2}(SbW_9O_{33})_2]^{7-}$ (Figures S1 and S2). In **{Zn_5_$Zn_{5.2}$}(2)**, the structure of the first polyanion $[Zn_5NaCl_3(H_2O)_4(SbW_9O_{33})_2]^{10-}$ has five Zn^{2+} centers and one vacancy in the Zn_5 belt with idealized C_{2v} symmetry (Figure 1c, Figure S2). The second polyanion $[Zn_{5.2}Na_{0.8}(H_2O)_{5.2}(SbW_9O_{33})_2]^{7-}$ with a $Zn_{5.2}$-TM cluster is identical to the respective second unit of **(1a** or **1b)**. The structure of $[Zn_{5.2}Na_{0.8}(H_2O)_{5.2}(SbW_9O_{33})_2]^{7-}$ contains four Zn^{2+} atoms (Zn5, Zn6, Zn5a, Zn6a) with one terminal water ligand comprising two binary units of square pyramids $[ZnO_4(H_2O)]$. The sites between these pyramid pairs exhibit positional disorder with site occupancies of 0.6 (Zn7) and 0.4 (Na3), respectively (Figure 1c).

The Zn_6-TM core of **Zn6(3a)** closely resembles the hexagonal $[Zn_6Cl_6O_{12}]$ ring of **Zn6(3b)**. Unlike (**3b**), the two Zn atoms (Zn2 and Zn2c) are bound to either one terminal water molecule (O33) or one terminal chloride ligand (Cl2) in **(3a)**, leading to the average formation of a $[Zn_6Cl_5(H_2O)O_{12}]^{17-}$ hexagonal Zn_6 core (Figure 1c, Figure S3).

In the Zn_5-TM core of **Zn_5(4)**, Zn1/Zn1a with one terminal Cl ligand and Zn2/Zn2a with one terminal water form two binary Zn moieties via adjacent edge-sharing $[ZnO_4Cl]$ and $[ZnO_4(H_2O)]$ square pyramids, while the remaining two sites between these Zn double units exhibit positional disorder (Figure 1c and Figure S4).

The polyanions of **Zn_5(5a)** and **Zn_5(5b)** consist of five adjacent Zn atoms while one Na^+ ion occupies the remaining site (Figure 1c and Figure S5 for **Zn_5(5a)**; Figure 1c and Figure S6 for **Zn_5(5b)**). The three Zn atoms (Zn1, Zn3 and Zn5) carrying a terminal water molecule are separated by Zn2 and Zn4 atoms coordinated with one monodentate acetate in **Zn_5(5a)**, while Zn5 in **Zn(5b)** binds to one chloride ligand, other than the terminal water in **Zn(5a)**.

The Zn_4-TM core of **Zn_4(6a)** differs from the {Zn_4} polyanion in {**Zn_4_$Zn_{5.2}$**}**(1a)** through one monodentate acetate ligand coordinating to Zn2 other than terminal water which leads to symmetry reduction (C_{2v} to C_s) (Figure 1c and Figure S7). The polyanions of **Zn_4(6b)** and **Zn_4(6c)** incorporate four zinc ions, which are not equivalent (Figure 1c and Figure S8 for **Zn_4(6b)**, Figure 1c and Figure S9 for **Zn_4(6c)**). Three of the Zn centers (Zn1, Zn3, and Zn4) carry a Cl ligand, whereas the fourth center Zn2 is connected to an acetate ligand in **(6b)** or to a water molecule in **(6c)** (Figure 1c). The enantiomers POMs **(6b)** and **(6c)** crystallize in the chiral space group $P2_12_12_1$. Neighboring sandwich-type polyanions are connected via additional Na^+ linkers into left- or right-handed helical chains that are further assembled into chiral 3D open frameworks (Figure S11).

The last newly characterized polyanion among the series, **$Zn_{3.5}$(7)**, differs from the known Zn_3-containing polyanion $[Zn_3Na_3(H_2O)_9(SbW_9O_{33})_2]^{9-}$ **Zn_3(8)** with idealized D_{3h} symmetry (Figure 1c and Figure S10 for **$Zn_{3.5}$(7)**; Figure S12a for **Zn_3(8)**): (a) only Zn4 is attached to a water molecule, whereas the remaining two Zn centers (Zn1 and Zn3) carry a Cl ligand; (b) the connecting positions between Zn1 and Zn3 atoms exhibit positional disorder (0.5 (Zn2) and 0.5 (Na3)).

Bond valence sum calculations (BVS) values of W, Sb, Zn and Na for all the compounds indicate no changes of the expected oxidation states of the metal ions (Tables S4-S6).

Phase purity of compounds (**(1a, 1b)**, **(3b)**, **(5a)**, **(5b)**, **(6a)**, **(6b)**, **(6c)**, **(7)**, and **(8)**) was confirmed with PXRD measurements (Figures S13-S22), and the presence of mixtures was excluded for **(2)**, **(3a)**, and **(4)**. The composition of all compounds was furthermore verified by elemental and thermogravimetric analyses which are in good agreement with X-ray crystallographic data (cf. Experimental section in the SI and Figure S23). Further details on the UV/Vis-, FT-IR-, and Raman spectroscopic characterization as well as the electrochemical properties of the Zn/Sb-POM family can be found in the Supporting Information (Figures S24 - S27, Table S7).

Table S1. Crystallographic data for compounds **Zn_4_$Zn_{5.2}$ (1a, 1b)**, **Zn_5_$Zn_{5.2}$ (2)**, and **Zn_6 (3a)**.

	Zn_4_$Zn_{5.2}$ (1a)	**Zn_4_$Zn_{5.2}$ (1b)**	**Zn_5_$Zn_{5.2}$ (2)**	**Zn_6 (3a)**
empirical formula	$Na_{9.4}O_{155.1}Sb_3W_{27}Zn_{7.6}$	$Na_{3.4}O_{155.6}Sb_3W_{27}Zn_{7.6}$	$Cl_6Na_{10.8}O_{186.2}Sb_4W_{36}Zn_{11.2}$	$Cl_{2.5}Na_2O_{55.5}SbW_9Zn_3$
formula weight (g·mol^{-1})	8523.72	8393.78	11277.94	2995.11
temperature (K)	183(2) K	183(2) K	183(2) K	183(2) K
wavelength (Å)	0.71073	0.71073	0.71073	0.71073
crystal system, space group	triclinic, *P-1*	triclinic, *P-1*	monoclinic, $P\,2_1/m$	monoclinic, *I 2/m*
a (Å)	18.9374(3)	18.4894(4)	17.9505(5)	13.8088(3)
b (Å)	19.3606(3)	19.0382(4)	29.1987(7)	22.2457(6)
c (Å)	23.4938(4)	22.9996(5)	19.9727(6)	18.8037(7)
α (deg)	97.481(1)	95.6868(18)	90	90.00
β (deg)	106.936(2)	111.139(2)	111.596(3)	91.711(2)
γ (deg)	114.482(2)	113.156(2)	90	90.00
volume (Å^3)	7181.1(2)	6663.3(2)	9733.5(5)	5773.7(3)
Z	2	2	2	4
abs. coeff. (mm^{-1})	23.471	25.274	23.282	19.768
density (calcd.) (Mg·m^{-3})	3.942	4.184	3.848	3.446
F(000)	7446	7322	9829	5262
crystal size (mm^3)	0.37 × 0.10 × 0.08	0.28× 0.08× 0.06	0.32 × 0.15 × 0.08	0.42 × 0.22 × 0.18
goodness-of-fit on F^2	1.036	1.044	1.044	1.099
$R_1[I > 2\sigma(I)]$	0.0552	0.0700	0.0623	0.0459
$wR_2\ [I > 2\sigma(I)]$	0.1460	0.1486	0.1637	0.1114

$R_1 = \sum(Fo - Fc)/\sum Fo$ *and* $wR_2 = \{\sum w(Fo^2 - Fc^2)^2/\sum w(Fo^2)^2\}^{1/2}$

Table S2. Crystallographic data for compounds **Zn$_6$ (3b)**, **Zn$_5$ (4)**, **Zn$_5$ (5a)**, and **Zn$_5$ (5b)**.

	Zn$_6$ (3b)	**Zn$_5$ (4)**	**Zn$_5$ (5b)**	**Zn$_5$ (5a)**
empirical formula	$Cl_6N_{12}O_{82}Sb_2W_{18}Zn_6$	$Cl_2Na_3O_{104}Sb_2W_{18}Zn_5$	$C_4ClNa_7O_{110}Sb_2W_{18}\ Zn_5$	$C_4Na_8O_{102}Sb_2W_{18}Zn_5$
formula weight (g·mol^{-1})	5637.84	5683.52	5884.07	5743.61
temperature (K)	183(2) K	183(2) K	183(2) K	183(2) K
wavelength (Å)	0.71073	0.71073	0.71073	0.71073
crystal system, space group	cubic, *Pa-3*	monoclinic, $P2_1/n$	triclinic, *P-1*	triclinic, *P-1*
a (Å)	20.4570(2)	13.1622(2)	14.6516(2)	12.8845(2)
b (Å)	20.4570(2)	18.4520(2)	16.9215(3)	17.2672(2)
c (Å)	20.4570(2))	17.8549(2)	21.8451(3)	24.7811(3)
α (deg)	90	90.00	85.3900(10)	109.0320(10)
β (deg)	90	90.0400(10)	85.8240(10)	92.3630(10)
γ (deg)	90	90.00	66.0200(10)	106.6400(10)
volume (Å^3)	8561.03(14)	4336.40(9)	4927.72(13)	4938.19(11)
Z	4	2	2	2
abs. coeff. (mm^{-1})	26.640	25.940	22.828	22.746
density (calcd.) (Mg·m^{-3})	4.374	4.353	3.966	3.863
F(000)	9824	4966	5164	5024
crystal size (mm^3)	0.11 × 0.05 × 0.05	0.21× 0.20 × 0.18	0.35 × 0.18× 0.15	0.35 × 0.21× 0.15
goodness-of-fit on F^2	0.926	1.054	1.085	1.093
$R_1[I > 2\sigma(I)]$	0.0375	0.0397	0.0394	0.0476
$wR_2\ [I > 2\sigma(I)]$	0.0652	0.0890	0.1027	0.1348

$R_1 = \sum(Fo - Fc)/\sum Fo$ *and* $wR_2 = \{\sum w(Fo^2 - Fc^2)^2/\sum w(Fo^2)^2\}^{1/2}$

Table S3. Crystallographic data for compounds **Zn_4 (6a)**, **Zn_4 (6b)**, **Zn_4 (6c)**, and **$Zn_{3.5}$ (7)**.

	Zn_4 (6a)	**Zn_4 (6b)**	**Zn_4 (6c)**	**$Zn_{3.5}$ (7)**
empirical formula	$CNa_9O_{100}Sb_2W_{18}Zn_4$	$C_2Cl_3N_5Na_{6.87}O_{99.5}Sb_2W_{18}Zn_{4.13}$	$Cl_3N_4Na_9O_{87}Sb_2W_{18}Zn_4$	$Cl_2Na_9O_{97.5}Sb_2W_{18}Zn_{3.5}$
formula weight (g·mol^{-1})	5633.20	5773.14	5575.58	5619.41
temperature (K)	183(2) K	183(2) K	183(2) K	183(2) K
wavelength (Å)	0.71073	0.71073	0.71073	0.71073
crystal system, space group	triclinic, *P-1*	orthorhombic, $P2_12_12_1$	orthorhombic, $P2_12_12_1$	triclinic, *P-1*
a (Å)	12.9159(2)	15.3168(5)	19.3332(4)	13.2947(3)
b (Å)	16.1825(2)	24.8457(9)	19.3423(8)	17.9950(3)
c (Å)	22.6036(3)	26.740(3)	27.2404(12)	21.0745(4)
α (deg)	104.3200(10)	90.00	90	77.724(2)
β (deg)	96.6540(10)	90.00	90	85.282(2)
γ (deg)	105.8740(10)	90.00	90	68.877(2)
volume (Å^3)	4316.84(10)	10176.1(12)	10186.5(7)	4595.44(16)
Z	2	4	4	2
abs. coeff. (mm^{-1})	25.750	21.951	21.890	24.116
density (calcd.) (Mg·m^{-3})	4.374	3.768	3.636	4.061
F(000)	4918	10110	9712	4904
crystal size (mm^3)	0.26 × 0.10 × 0.05	0.38× 0.35 × 0.25	0.39 × 0.13 × 0.11	0.15 × 0.13 × 0.05
goodness-of-fit on F^2	0.959	1.048	1.051	1.028
$R_1[I > 2\sigma(I)]$	0.0298	0.0545	0.0703	0.0450
$wR_2 [I > 2\sigma (I)]$	0.0658	0.1320	0.1466	0.1132

$R_1 = \sum(Fo - Fc)/\sum Fo$ and $wR_2 = \{\sum w(Fo^2 - Fc^2)^2/\sum w(Fo^2)^2\}^{1/2}$

Table S4. Bond valence sums (BVS) for **Zn_4_$Zn_{5.2}$ (1a, 1b)**, **Zn_5_$Zn_{5.2}$ (2)**, and **Zn_6 (3a)**.

Zn_4_$Zn_{5.2}$ (1a)

Zn1	2.1010	Zn2	1.9684	Zn3	2.1795	Zn4	2.0618
Zn5	2.1371	Zn6	2.0381	Zn7	1.9517	Sb1	2.9534
Sb2	2.9977	Sb3	2.9904	W1	6.2422	W2	5.9633
W3	6.0282	W4	6.0082	W5	6.1323	W6	5.8627
W7	6.1017	W8	6.0207	W9	6.2158	W10	6.0895
W11	6.1273	W12	6.1701	W13	6.0662	W14	5.9996
W15	6.0858	W16	6.1066	W17	6.0525	W18	6.1959
W19	6.2193	W20	6.1455	W21	6.0388	W22	5.9551
W23	5.9749	W24	5.9749	W25	6.0989	W26	5.9964
W27	5.9725	Na1	1.1145	Na2	1.0617		

Zn_4_$Zn_{5.2}$ (1b) (disordered W atoms were excluded)

Zn1	2.1002	Zn2	2.1217	Zn3	1.9522	Zn4	2.1247
Zn5	2.0070	Zn6	1.8876	Zn7	2.0886	Sb1	3.0084
Sb2	2.9870	Sb3	3.0164	W1	6.0890	W2	6.0189
W3	6.2695	W4	6.0633	W5	6.1355	W6	5.9091
W7	6.1307	W8	6.1415	W9	5.8985	W11	6.1273
W12	6.2807	W13	6.2866	W14	6.0984	W19	6.0302
W20	5.9560	W21	6.0842	W25	6.1268	W26	6.2898
W27	6.1015	Na1	1.1165	Na2	1.0814	Na1	1.1165

Zn_5 $Zn_{5.2}$ (2)

Zn1	2.0657	Zn2	2.0306	Zn3	2.3509	Zn4	1.9204
Zn5	2.3730	Zn6	2.2383	Na1	1.0062	Sb1	3.1525
Sb2	2.9597	Sb3	2.8858	W1	6.1551	W2	6.1516
W3	5.9077	W4	6.1594	W5	6.1781	W6	6.0161
W7	6.0577	W8	6.2436	W9	6.1767	W10	6.2448
W11	6.2129	W12	5.7972	W13	6.0636	W14	6.0324
W15	6.0355	W16	6.0021	W17	6.1377	W18	6.2369
W19	6.3357	Sb4					

Zn6 (3a)

Zn1	1.9642	Zn2	2.0202	W1	5.9731	W2	5.9884
W3	5.9459	W4	5.9885	W4	5.9515	Sb1	3.1322
Cl1	0.5059	Cl2	0.4705				

Table S5. Bond valence sums (BVS) for **Zn_6 (3b)**, **Zn_5 (4)**, **Zn_5 (5a)**, and **Zn_5 (5b)**.

Zn6 (3b)

Zn1	1.9627	Cl1	0.5367	Sb1	3.1367	W1	6.1020
W2	6.0204	W3	6.0348				

Zn_5 (4)

Zn1	2.0178	Zn2	1.9872	Zn3	1.7560	Na1	1.3497
Sb1	2.9161	W1	6.1090	W2	6.0546	W3	6.1400
W4	6.0417	W5	6.0612	W6	6.0045	W7	6.0436
W8	6.1674	W9	6.1058				

Zn_5 (5a)

Zn1	2.1034	Zn2	2.0178	Zn3	2.1122	Zn4	1.9260
Zn5	1.8177	Na1	1.0432	Sb1	2.9202	Sb2	2.9508
W1	6.1802	W2	6.1738	W3	6.0888	W4	6.0681
W5	6.0933	W6	6.1144	W7	6.0896	W8	6.1000
W9	6.0492	W10	6.1078	W11	6.2000	W12	6.1056
W13	6.1329	W14	6.0299	W15	6.1269	W16	5.9737
W17	6.3062	W18	6.0397				

Zn_5 (5b)

Zn1	2.1359	Zn2	2.0035	Zn3	2.0795	Zn4	1.9677
Zn5	2.1490	Na1	1.1157	Sb1	3.0728	Sb1	2.9375
W1	6.1151	W2	6.2581	W3	5.8676	W4	5.9575
W5	5.8611	W6	6.0404	W7	6.2257	W8	6.0343
W9	5.9265	W10	6.0034	W11	6.1007	W12	6.1411
W13	6.0847	W14	6.0483	W15	6.1621	W16	6.1164
W17	6.0603	W18	6.1490				

Table S6. Bond valence sums (BVS) for **Zn$_4$ (6a), Zn$_4$ (6b), Zn$_4$ (6c) and Zn$_{3.5}$ (7)**.

Zn$_4$ (6a)							
Zn1	2.1080	Zn2	1.9915	Zn3	2.1478	Zn4	2.1467
Na1	1.0400	Na2	1.0945	Sb1	2.9095	Sb2	2.9433
W1	6.0987	W2	6.0671	W3	6.0880	W4	6.0839
W5	6.1373	W6	6.1402	W7	6.0186	W8	6.0348
W9	6.0856	W10	6.1009	W11	6.1185	W12	6.1107
W13	6.0680	W14	6.0642	W15	6.0273	W16	6.1349
W17	6.0895	W18	6.1377				
Zn$_4$ (6b)							
Zn1	2.1349	Zn2	2.0124	Zn3	2.1953	Zn4	2.1896
Na1	1.0969	Na2	1.1675	Sb1	2.8644	Sb2	2.9082
W1	6.2356	W2	6.3261	W3	5.9509	W4	6.1529
W5	6.1161	W6	6.0460	W7	6.0194	W8	6.1544
W9	6.0335	W10	6.1179	W11	6.2375	W12	6.0638
W13	6.1188	W14	6.1882	W15	6.0471	W16	6.0904
W17	6.0457	W18	5.9521				
Zn$_4$ (6c)							
Zn1	2.0682	Zn2	1.8778	Zn3	2.1153	Zn4	2.1809
Na1	1.2616	Na2	1.2616	Sb1	3.0375	Sb2	3.0003
W1	6.4278	W2	6.2217	W3	6.1115	W4	6.2366
W5	6.0063	W6	6.0056	W7	6.0671	W8	6.1049
W9	5.9780	W10	6.0353	W11	6.4154	W12	5.9516
W13	6.1636	W14	6.2073	W15	6.3222	W16	5.7588
W17	6.0754	W18	6.4661				
Zn$_{3.5}$ (7)							
Zn1	2.1388	Zn2	2.1642	Zn3	2.0869	Na1	1.1366
Na1	1.0863	Na3	1.2036	Sb1	2.8193	Sb1	2.9409
W1	6.0831	W2	6.1839	W3	6.1642	W4	6.0607
W5	5.9553	W6	6.1527	W7	6.2057	W8	5.9830
W9	6.0342	W10	5.9933	W11	6.0925	W12	6.0026
W13	6.0757	W14	6.2384	W15	6.0351	W16	6.0412
W17	6.2023	W18	6.1435				

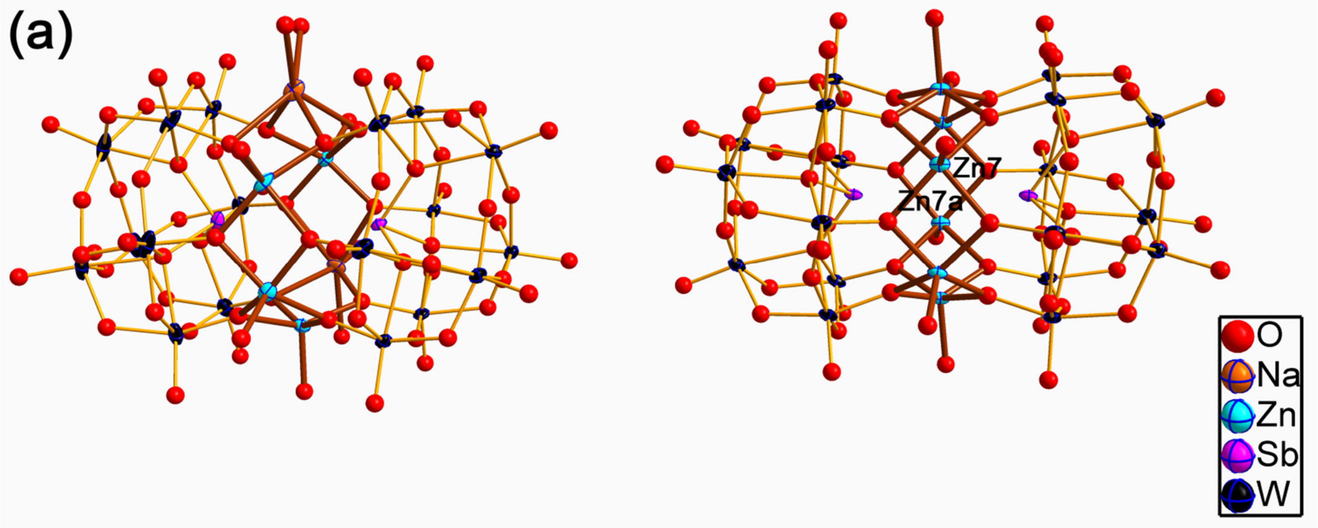

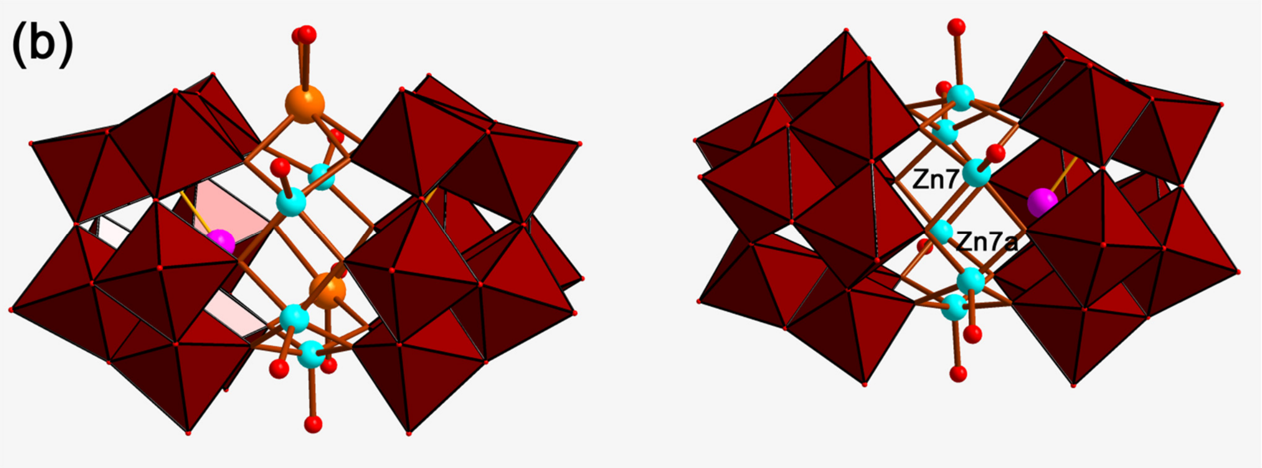

Figure S1. (a) Ball-and-stick representation of the polyoxoanion $[Zn_4Na_2(H_2O)_8(SbW_9O_{33})_2][Zn_{5.2}Na_{0.8}(H_2O)_{5.2}(SbW_9O_{33})_2]^{15-}$ **{Zn_4_$Zn_{5.2}$} (1a or 1b)** (thermal ellipsoids of heavy atoms at 50 % probability level; only the major site-occupancy of the disordered Zn7 (Na3) is shown for clarity in **(1a)**, symmetry codes: a, *-x, 1-y,1- z* for **(1a)**). (b) Polyhedral representation of the polyoxoanion **{Zn_4_$Zn_{5.2}$} (1a or 1b)** (color codes: WO_6 octahedra = red; Sb = pink; W = black; Zn = blue; Na = orange; O = red).

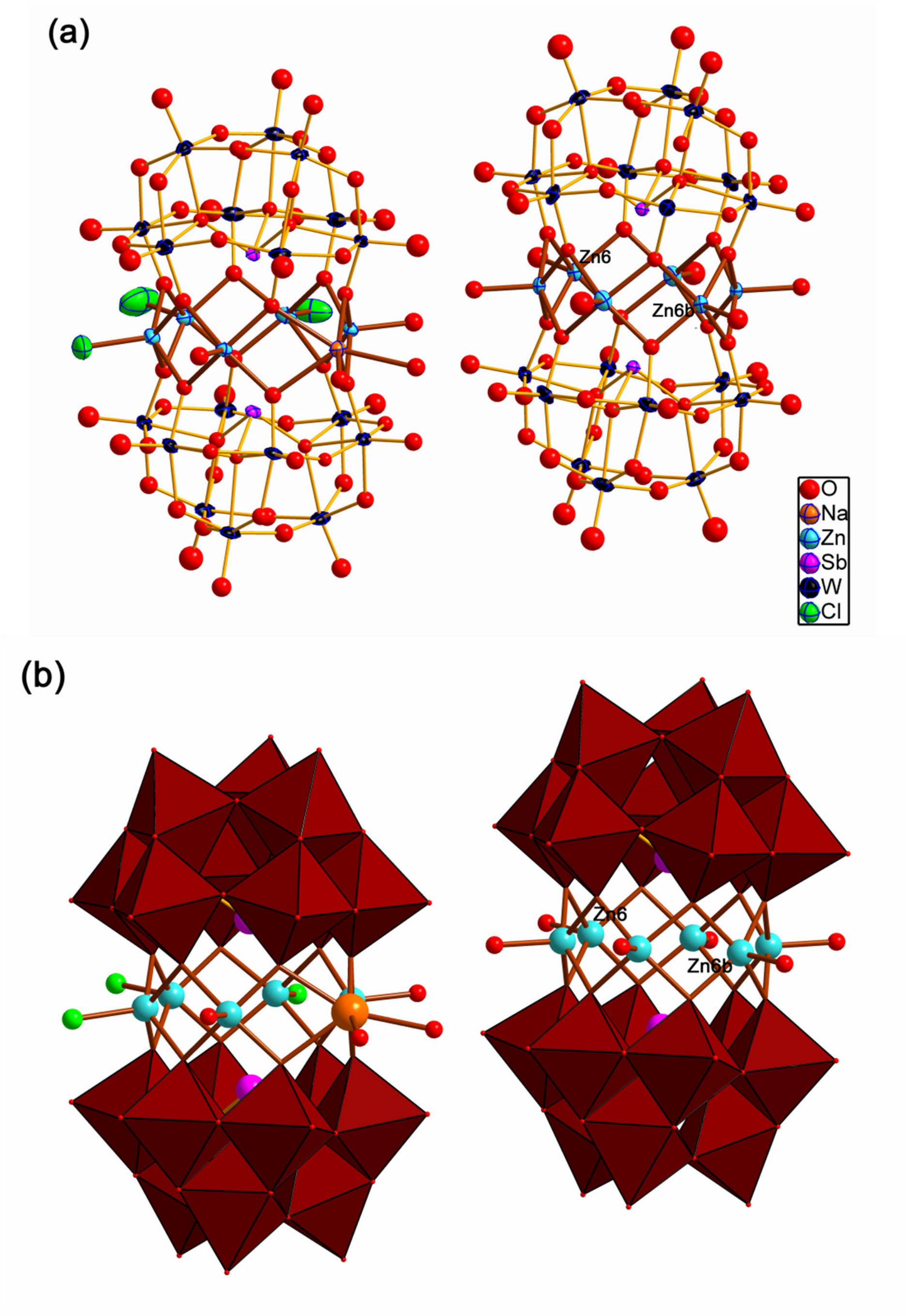

Figure S2. (a) Ball-and-stick representation of the polyoxoanion $\{[Zn_5NaCl_3(H_2O)_4(SbW_9O_{33})_2][Zn_{5.2}Na_{0.8}(H_2O)_{5.2}(SbW_9O_{33})_2]\}^{17-}$ **{Zn₅_Zn₅.₂} (2)** (thermal ellipsoids of heavy atoms at 50 % probability level, only major site-occupancy of the disordered Zn6 (Na2) is shown for clarity, symmetry codes: b, *1-x, 1-y, 1-z*). (b) Polyhedral representation of the polyoxoanion **{Zn₅_Zn₅.₂} (2)** (Color codes: WO_6 octahedra = red; Sb = pink; W = black; Zn = blue; Na = orange; O = red; Cl = green).

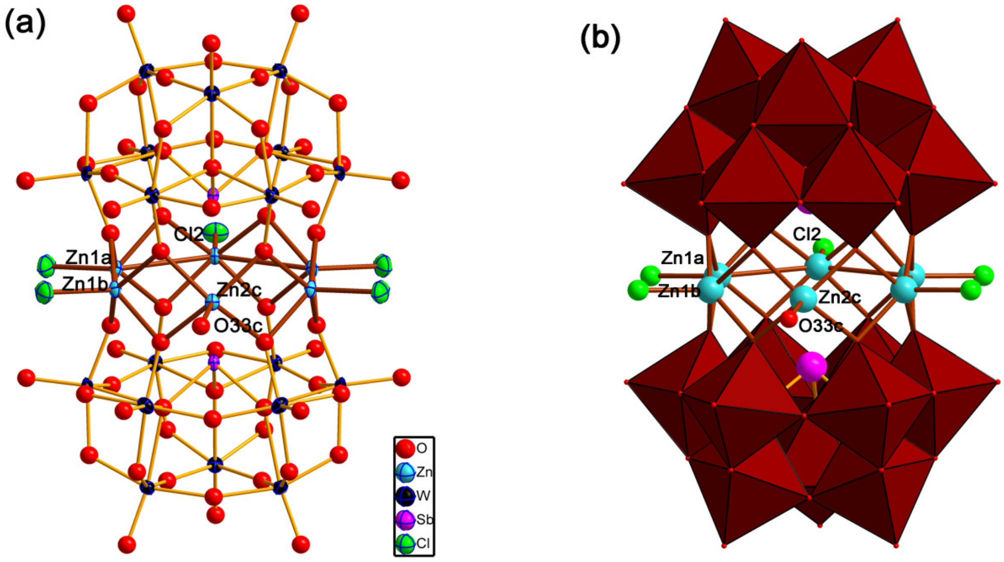

Figure S3. (a) Ball-and-stick representation of the polyoxoanion $[Zn_6(H_2O)Cl_5(SbW_9O_{33})_2]^{11-}$ **$\{Zn_6\}$ (3a)** (thermal ellipsoids of heavy atoms at 50 % probability level; Cl2 and O33c are site-occupancy disordered with the quarter-occupancies, symmetry codes: a, *x, -y, -z;* b, *-1-x, -y, -z;* c, *-1-x, y, -z*). (b) Polyhedral representation of the polyoxoanion **{Zn6} (3a)** (color codes: WO_6 octahedra = red; Sb = pink; W = black; Zn = blue; O = red; Cl = green).

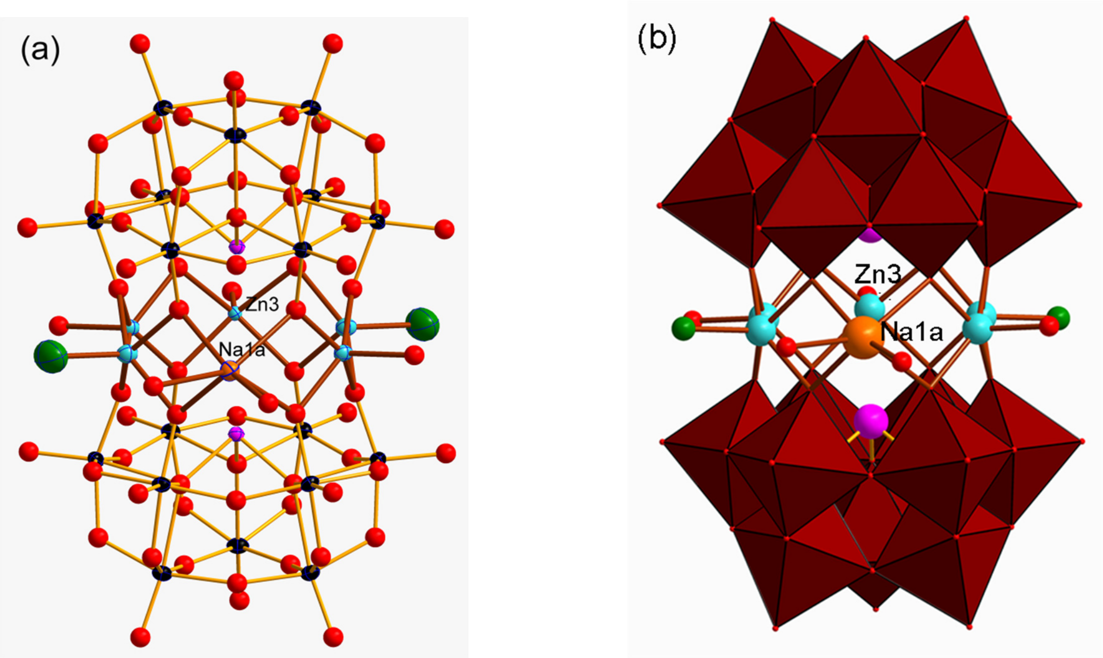

Figure S4. (a) Ball-and-stick representation of the polyoxoanion $[Zn_5Na(H_2O)_5Cl_2(SbW_9O_{33})_2]^{9-}$ **{Zn$_5$} (4)** (thermal ellipsoids of heavy atoms at 50 % probability level, half-occupancy position of the disordered Na1a (Zn3a) is shown for clarity, symmetry codes: a, 1-*x, -y, 1-z*). (b) Polyhedral representation of the polyoxoanion **{Zn5} (4)** (color codes: WO_6 octahedra = red; Sb = pink; W = black; Zn = blue; O = red; Cl = green).

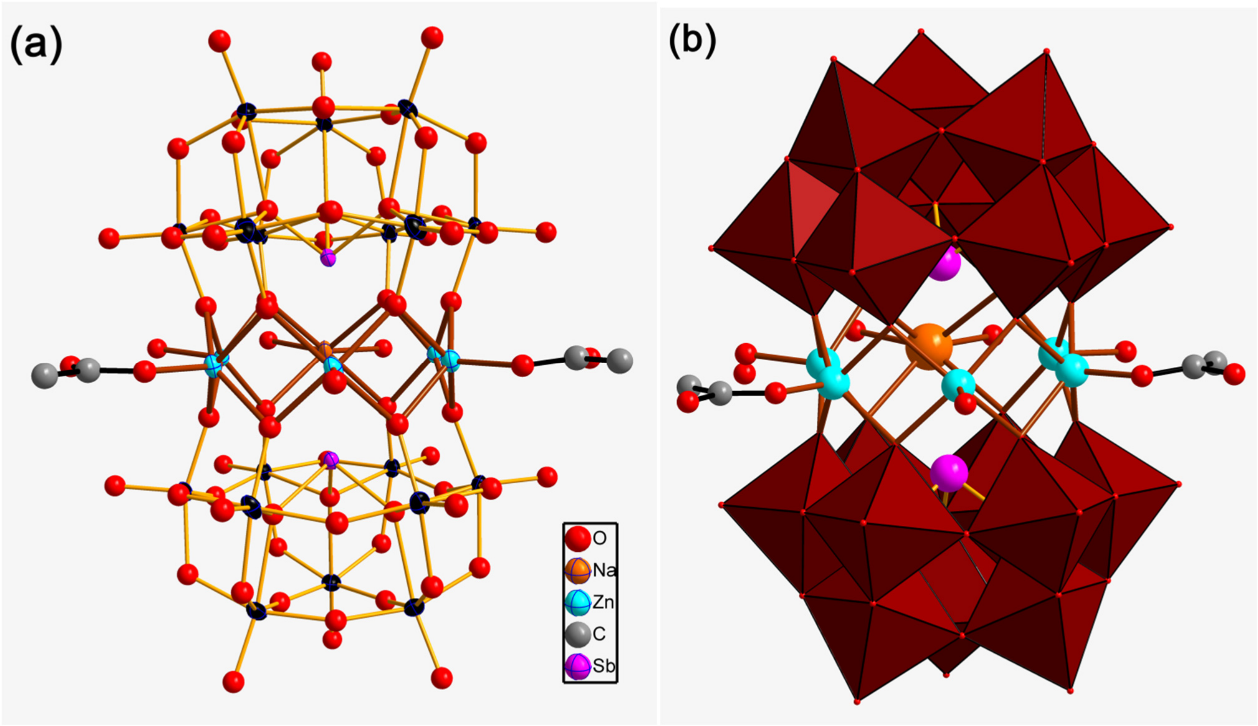

Figure S5. (a) Ball-and-stick representation of the polyoxoanion $[Zn_5Na(H_2O)_5(CH_3COO)_2(SbW_9O_{33})_2]^{9-}$ **{Zn$_5$} (5a)** (thermal ellipsoids of heavy atoms at 50 % probability level). (b) Polyhedral representation of the polyoxoanion **{Zn$_5$} (5a)** (color codes: WO_6 octahedra = red; Sb = pink; W = black; Zn = blue; Na = orange; O = red; C = grey).

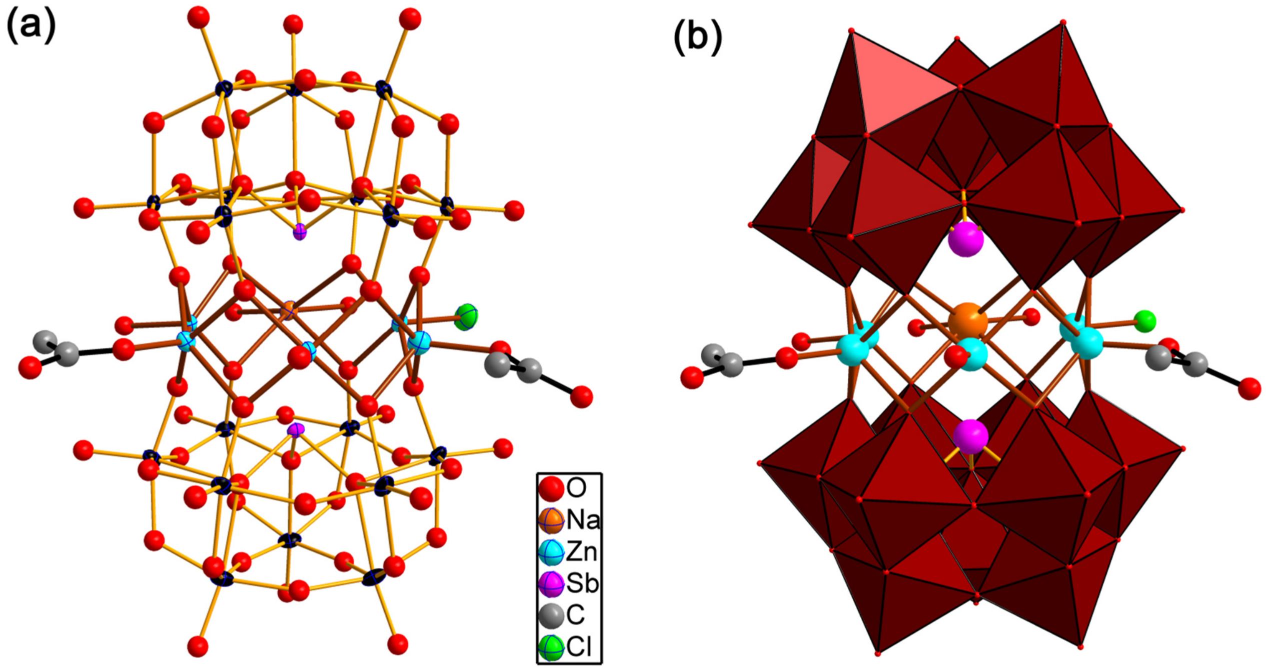

Figure S6. (a) Ball-and-stick representation of the polyoxoanion $[Zn_5Na(H_2O)_4Cl(CH_3COO)_2(SbW_9O_{33})_2]^{10-}$ **$\{Zn_5\}$ (5b)** (thermal ellipsoids of heavy atoms at 50 % probability level). (b) Polyhedral representation of the polyoxoanion **$\{Zn_5\}$ (5b)** (Color codes: WO_6 octahedra = red; Sb = pink; W = black; Zn = blue; Na = orange; O = red; Cl = green; C = grey).

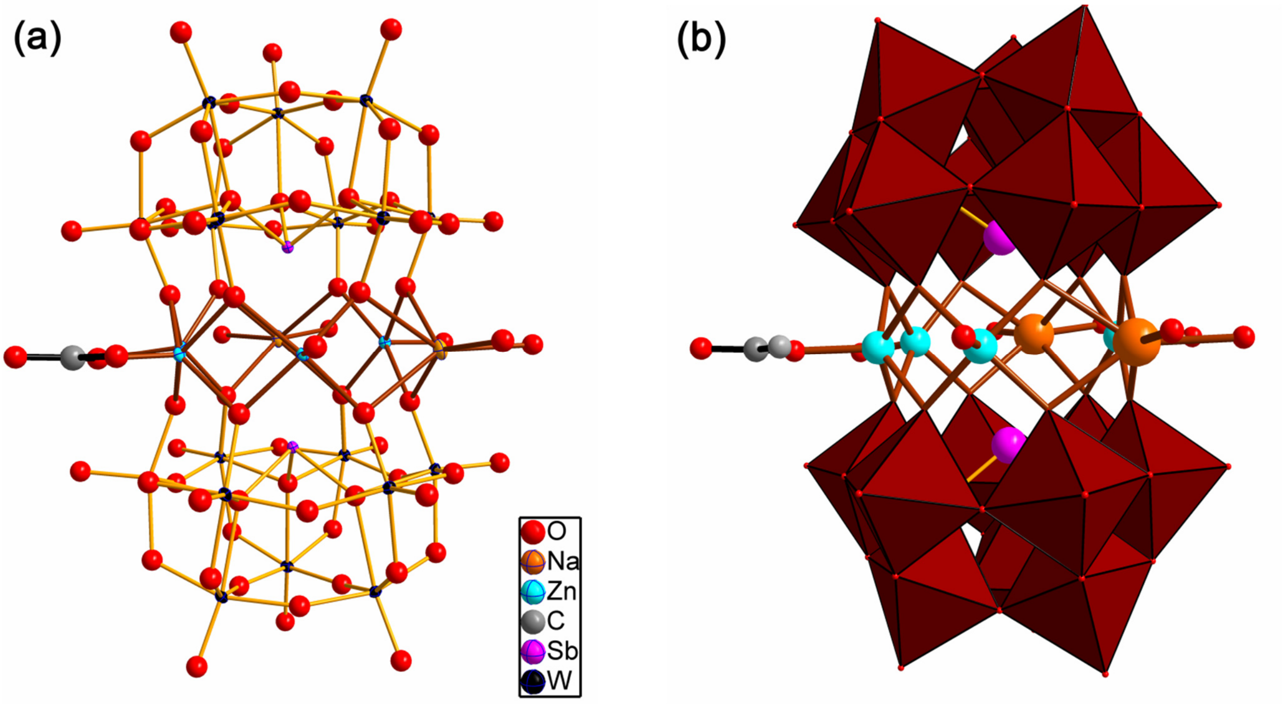

Figure S7. (a) Ball-and-stick representation of the polyoxoanion $[Zn_4Na_2(H_2O)_7(CH_3COO)(SbW_9O_{33})_2]^{9-}$ **{Zn$_4$} (6a)** (thermal ellipsoids of heavy atoms at 50 % probability level). (b) Polyhedral representation of the polyoxoanion **{Zn$_4$} (6a)** (color codes: WO_6 octahedra = red; Sb = pink; W = black; Zn = blue; Na = orange; O = red; C = grey).

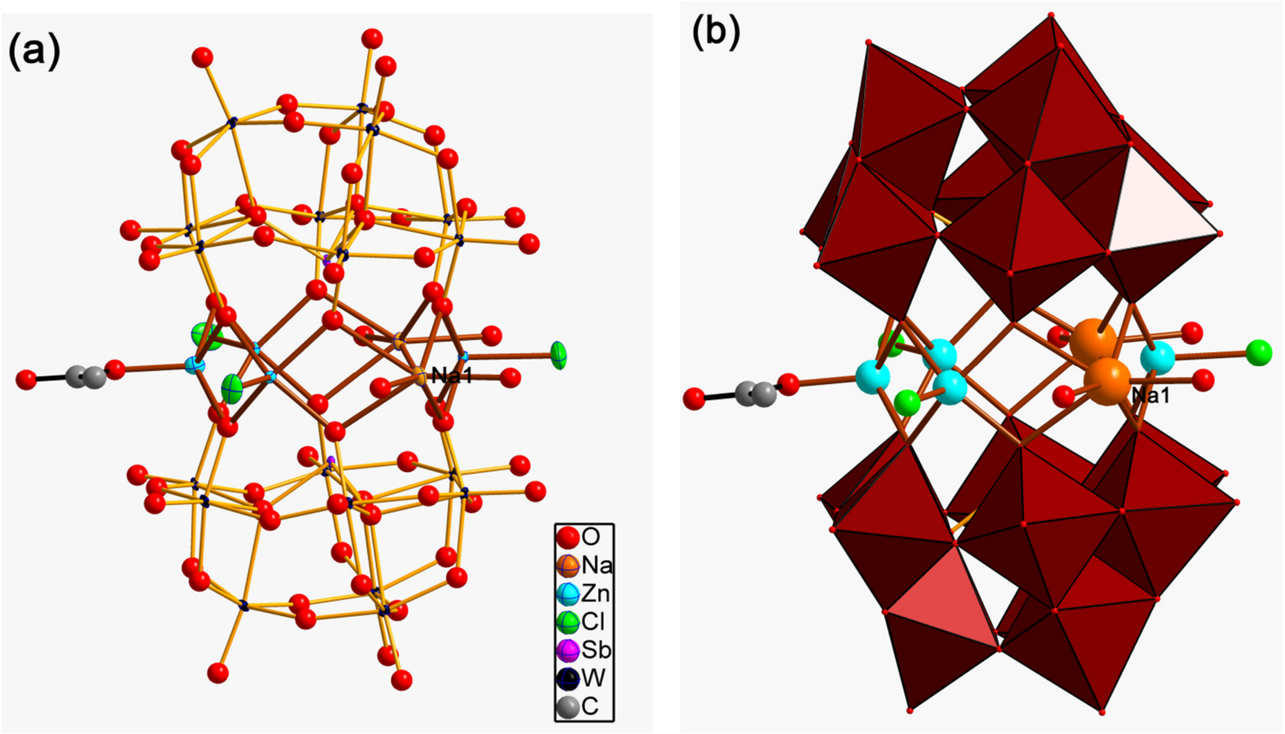

Figure S8. (a) Ball-and-stick representation of the polyoxoanion $[Zn_{4.1}Na_{1.9}Cl_3(H_2O)_7(CH_3COO)(SbW_9O_{33})_2]^{12-}$ **{Zn$_4$} (6b)** (thermal ellipsoids of heavy atoms at 50 % probability level; only the major site-occupancy of the disordered Na1 (Zn5) is shown for clarity). (b) Polyhedral representation of the polyoxoanion **{Zn$_4$} (6b)** (color codes: WO_6 octahedra = red; Sb = pink; W = black; Zn = blue; Na = orange; O = red; C = grey; Cl = green).

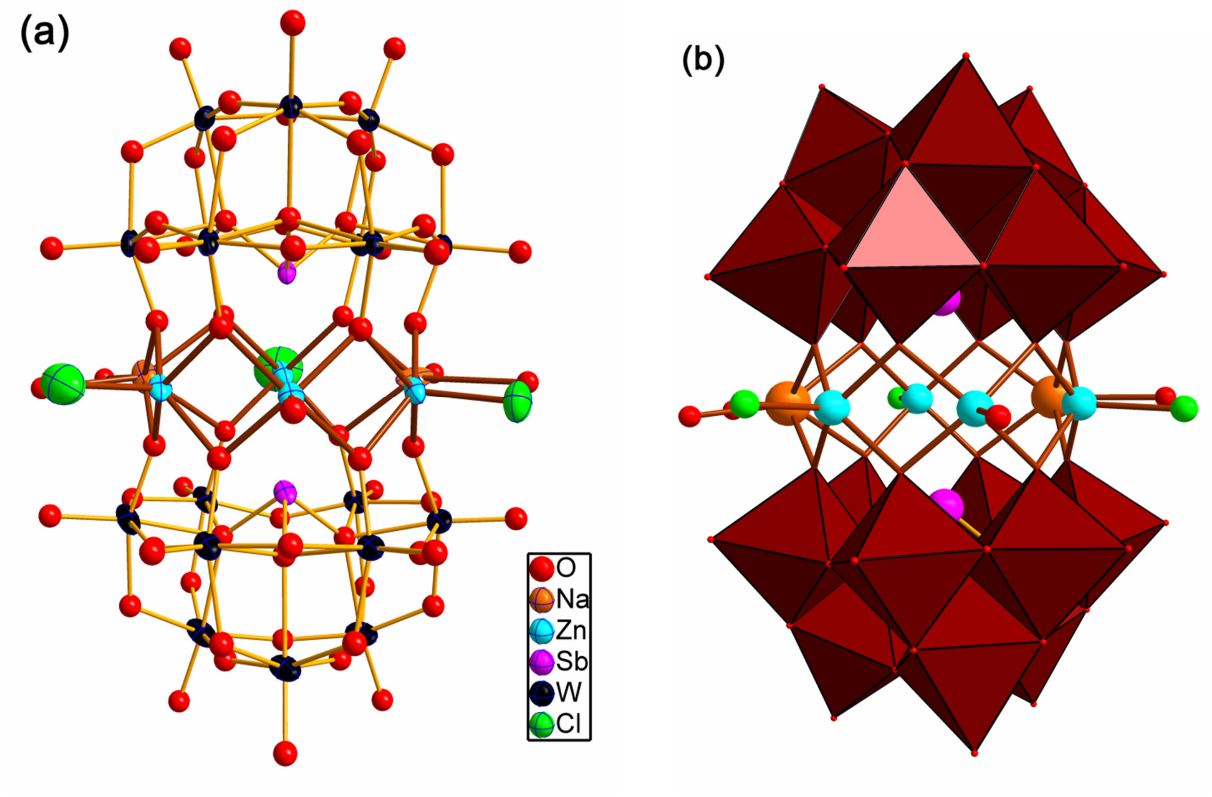

Figure S9. (a). Ball-and-stick representation of the polyoxoanion $[Zn_4Na_2Cl_3(H_2O)_5(SbW_9O_{33})_2]^{11-}$ **{Zn$_4$} (6c)** (thermal ellipsoids of heavy atoms at 50 % probability level). (b) Polyhedral representation of the polyoxoanion **{Zn$_4$} (6c)** (color codes: WO_6 octahedra = red; Sb = pink; W = black; Zn = blue; Na = orange; O = red; Cl = green).

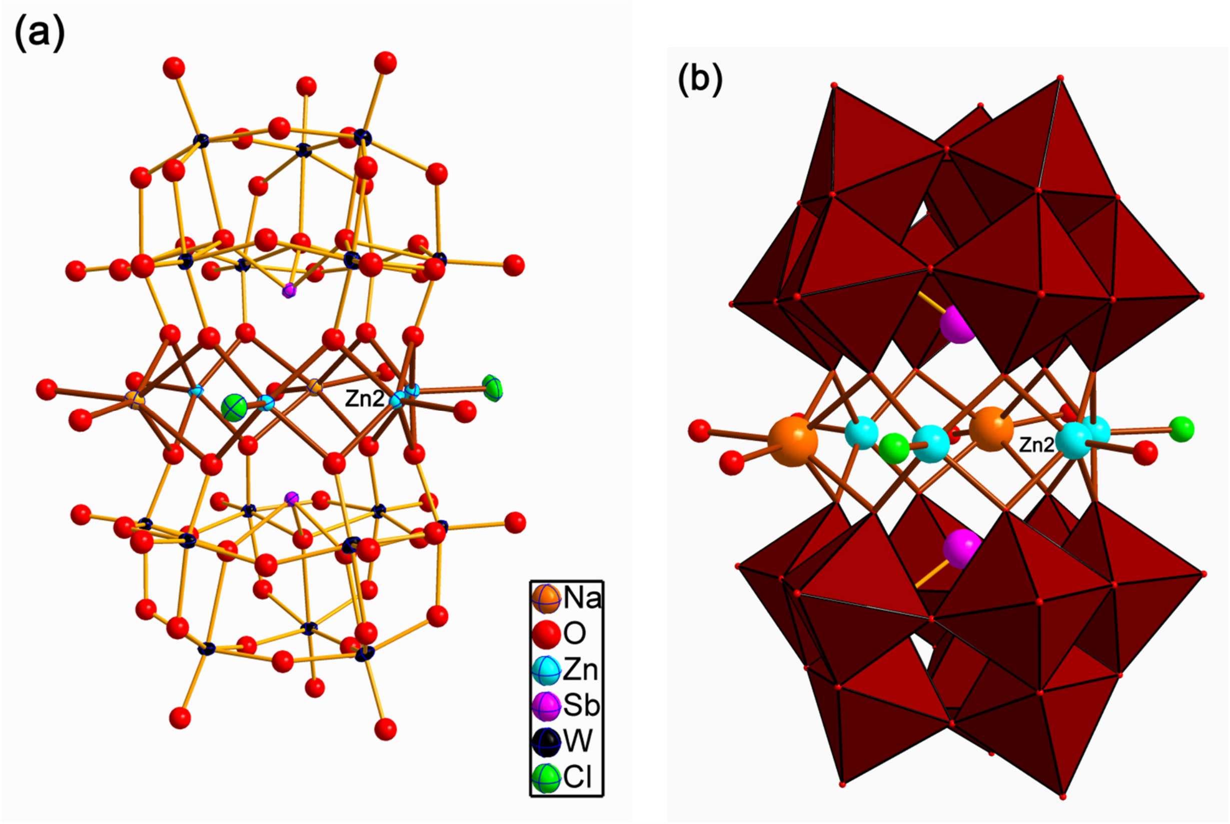

Figure S10. (a). Ball-and-stick representation of the polyoxoanion $[Zn_{3.5}Na_{2.5}Cl_2(H_2O)_6(SbW_9O_{33})_2]^{10-}$ **$\{Zn_{3.5}\}$ (7)** (thermal ellipsoids of heavy atoms at 50 % probability level; half-occupancy position of the disordered Zn2 (Na3) is shown for clarity). (b) Polyhedral representation of the polyoxoanion **$\{Zn_{3.5}\}$ (7)** (color codes: WO_6 octahedra = red; Sb = pink; W = black; Zn = blue; Na = orange; O = red; Cl = green).

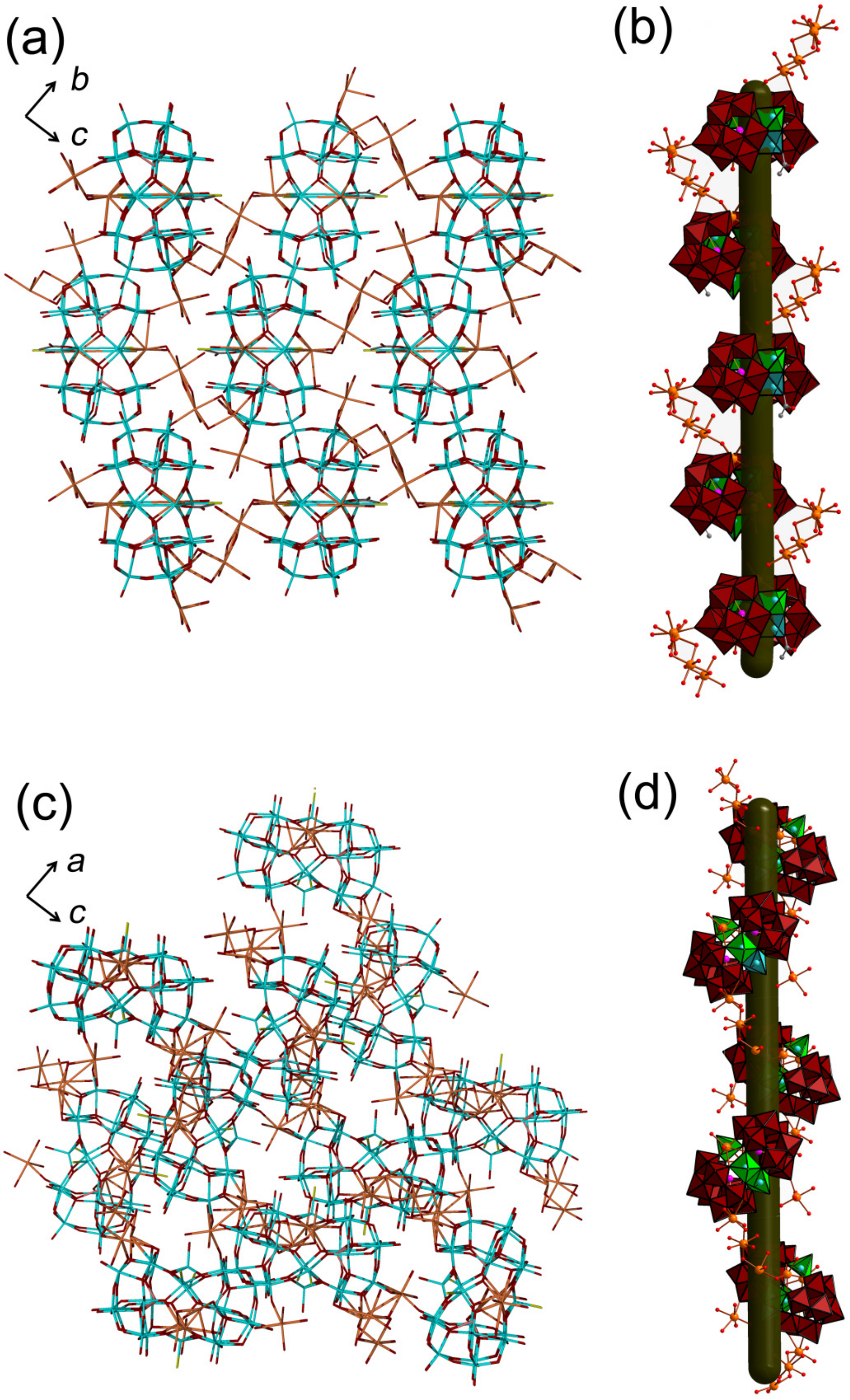

Figure S11. (a) 3D open-framework structure of **Zn_4 (6b)** shown along the *a* axis. (b) Left-handed helices in **Zn_4 (6b)**. (c) 3D open-framework structure of **Zn_4 (6c)** with view of the *ac* plane. (d) Right-handed helices in **Zn_4 (6c)**.

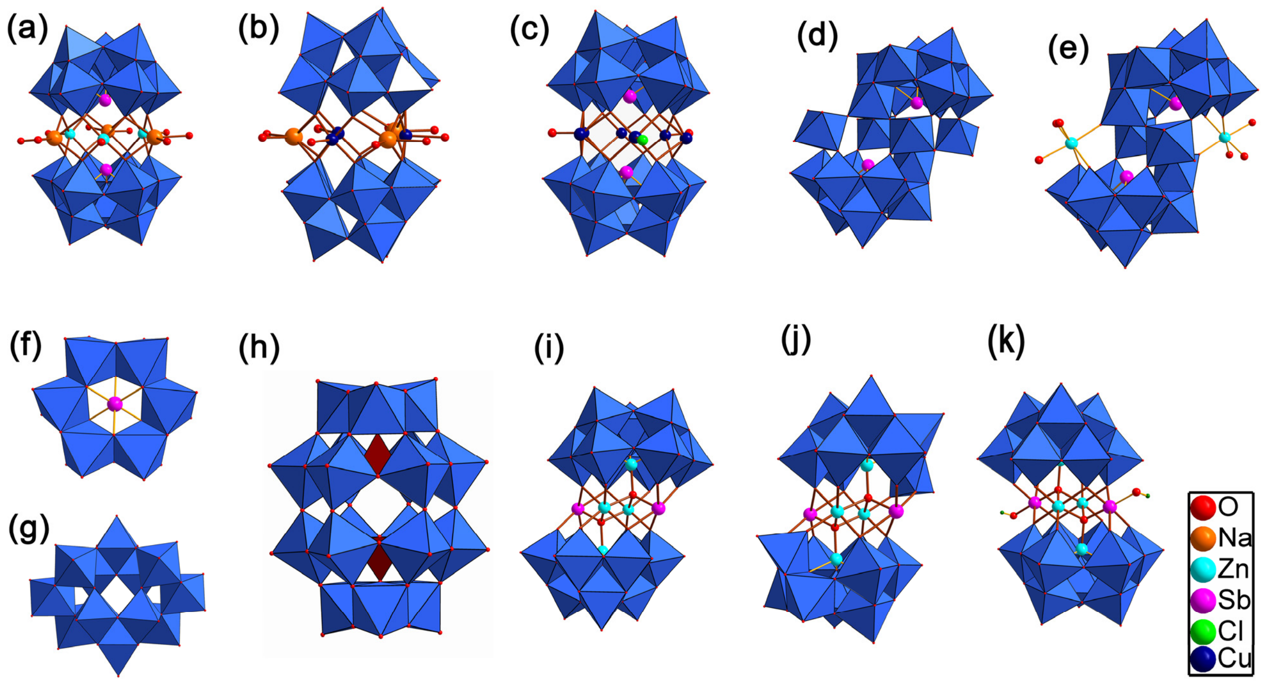

Figure S12. Polyhedral representations of (a) sandwich-type $[Zn_3Na_3(H_2O)_9(SbW_9O_{33})_2]^{9-}$ **{Zn₃(8)}**, (b) sandwich-type $[Cu_3Na_3(H_2O)_9(SbW_9O_{33})_2]^{9-}$ **{Cu₃}**, (c) sandwich-type $[Cu_6Cl(H_2O)_2(SbW_9O_{33})_2]^{7-}$ **{Cu₆}**, (d) *Krebs*-type $[Sb_2W_{22}O_{74}(OH)_2]^{12-}$, (e) *Krebs*-type $[Zn_2Sb_2W_{20}O_{70}]^{10-}$, (f) Sb(V)-substituted *Anderson*-type $[Sb^{V}W_6O_{24}]^{7-}$, (g) paratungstate $[H_2W_{12}O_{42}]^{10-}$, (h) Wells-Dawson polyoxometalate $[\alpha\text{-}P_2W_{18}O_{62}]^{6-}$, (i) and (j) sandwich-type $[\alpha/\beta\text{-}Zn_2Sb^{III}_2(ZnW_9O_{34})_2]^{14-}$ {α/β-Zn_2Sb_2 isomers}, (k) high valent Sb(V)-substituted sandwich-type $[\alpha\text{-}Zn_2Sb^{V}_2(OH)_2(ZnW_9O_{34})_2]^{12-}$, (color codes: WO_6 octahedra = light blue; PO_4 tetrahedra = brown; Sb = pink; Zn = sky blue; Cu = dark blue; Na = orange; O = red; Cl = green).

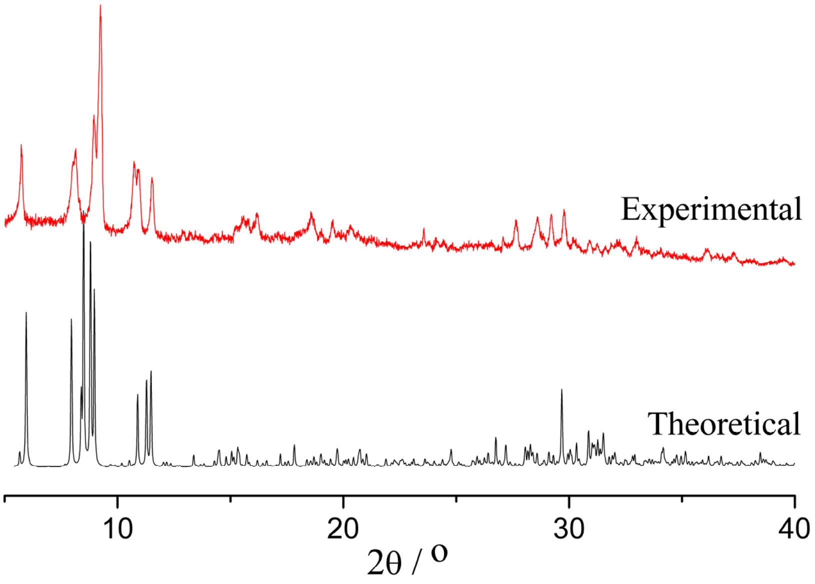

Figure S13. Powder X-ray diffraction (PXRD) pattern of bulk **Zn$_4$-Zn$_{5.2}$ (1a)** vs. calculated pattern. Intensity differences may be due to preferred orientation of the powder sample.

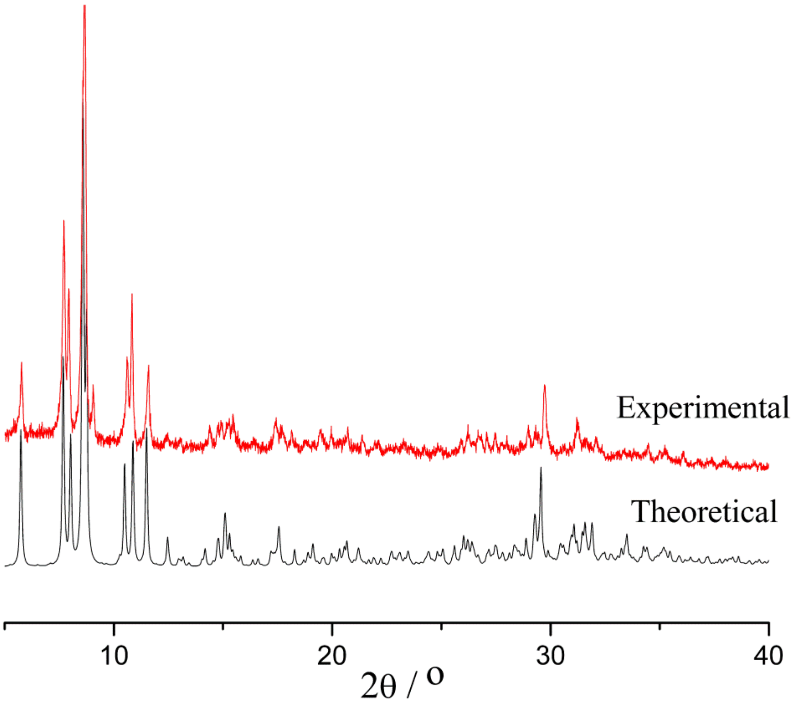

Figure S14. PXRD pattern of bulk **Zn$_4$-Zn$_{5.2}$ (1b)** vs. calculated pattern. Intensity differences may be due to preferred orientation of the powder sample.

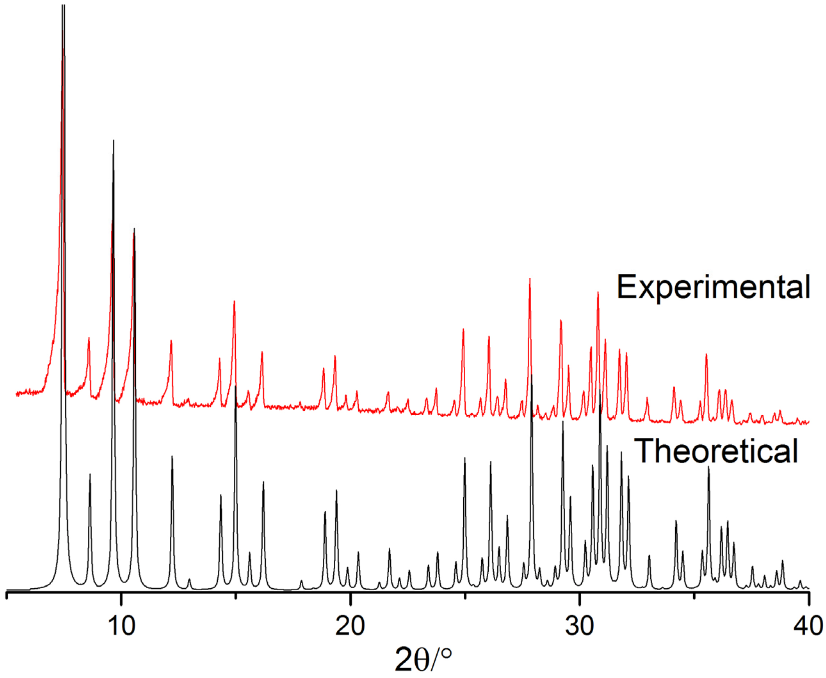

Figure S15. PXRD pattern of bulk **Zn_6 (3b)** vs. calculated pattern. Intensity differences may be due to preferred orientation of the powder sample.

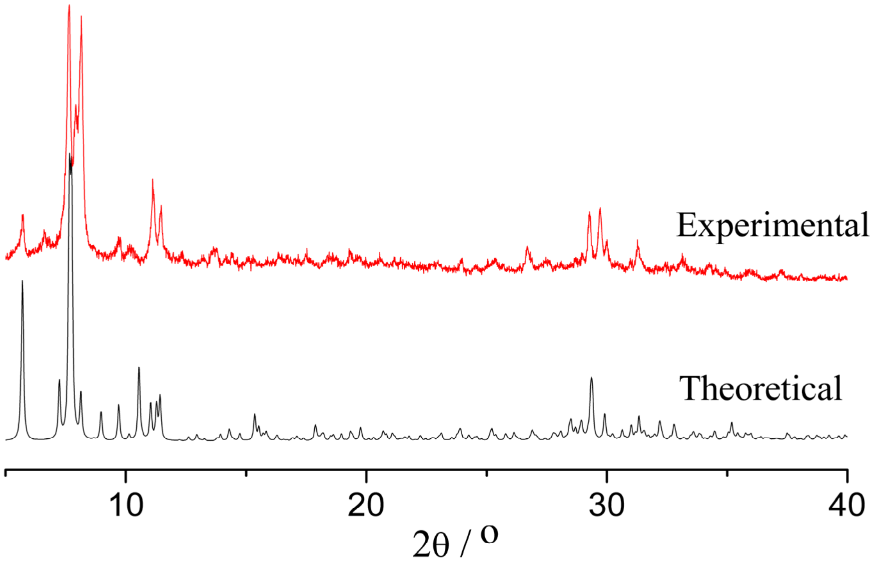

Figure S16. PXRD diffraction pattern of bulk **Zn_5 (5a)** vs. calculated pattern. Intensity differences may be due to preferred orientation of the powder sample.

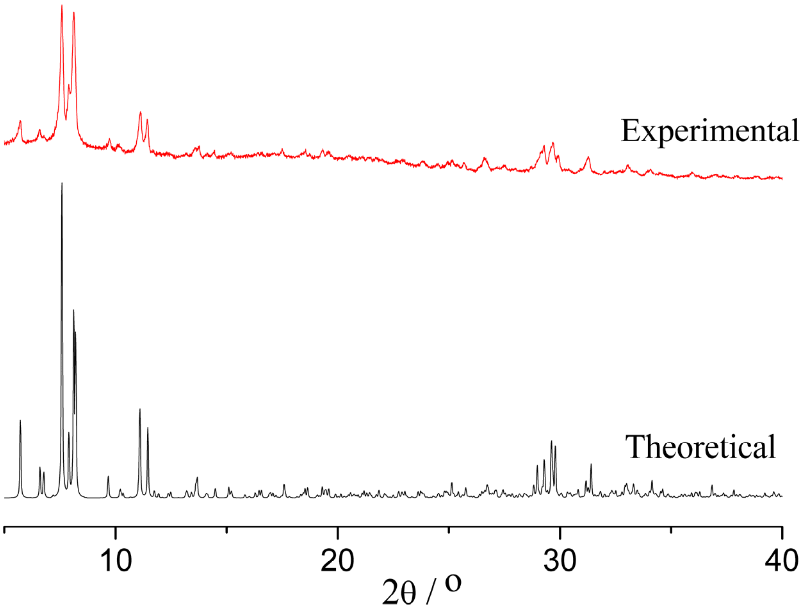

Figure S17. PXRD pattern of bulk **Zn$_5$ (5b)** vs. calculated pattern. Intensity differences may be due to preferred orientation of the powder sample.

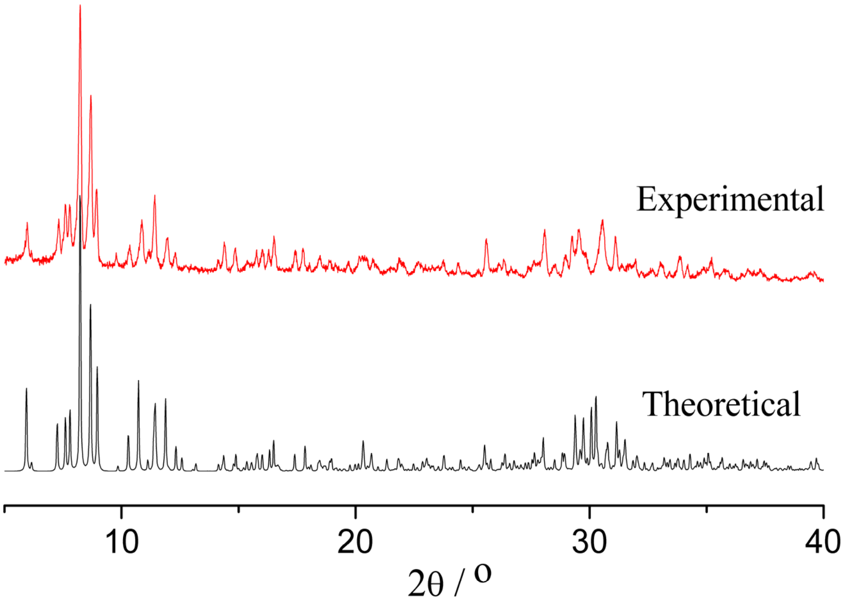

Figure S18. PXRD pattern of bulk **Zn$_4$ (6a)** vs. calculated pattern. Intensity differences may be due to preferred orientation of the powder sample.

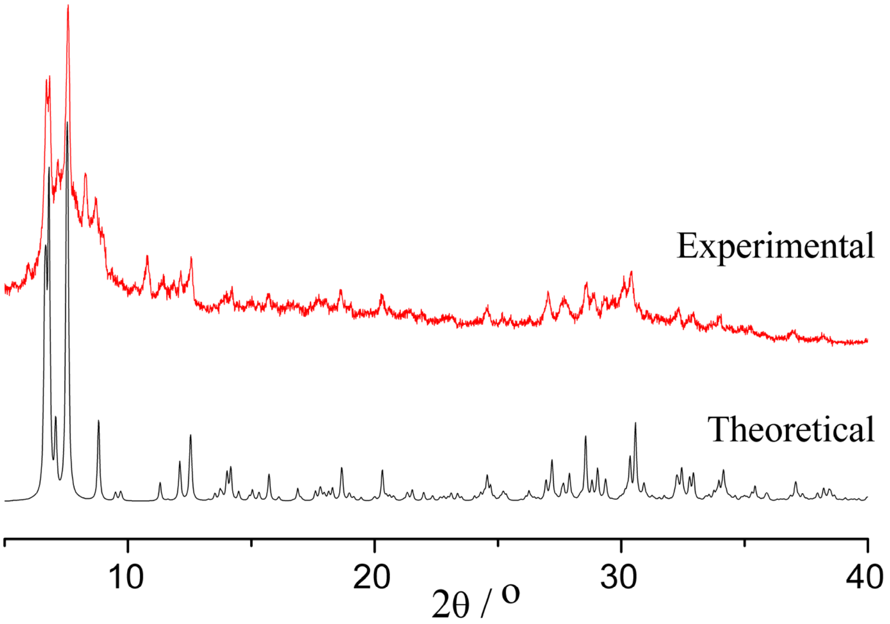

Figure S19. PXRD pattern of bulk **Zn$_4$ (6b)** vs. calculated pattern. Intensity differences may be due to preferred orientation of the powder sample.

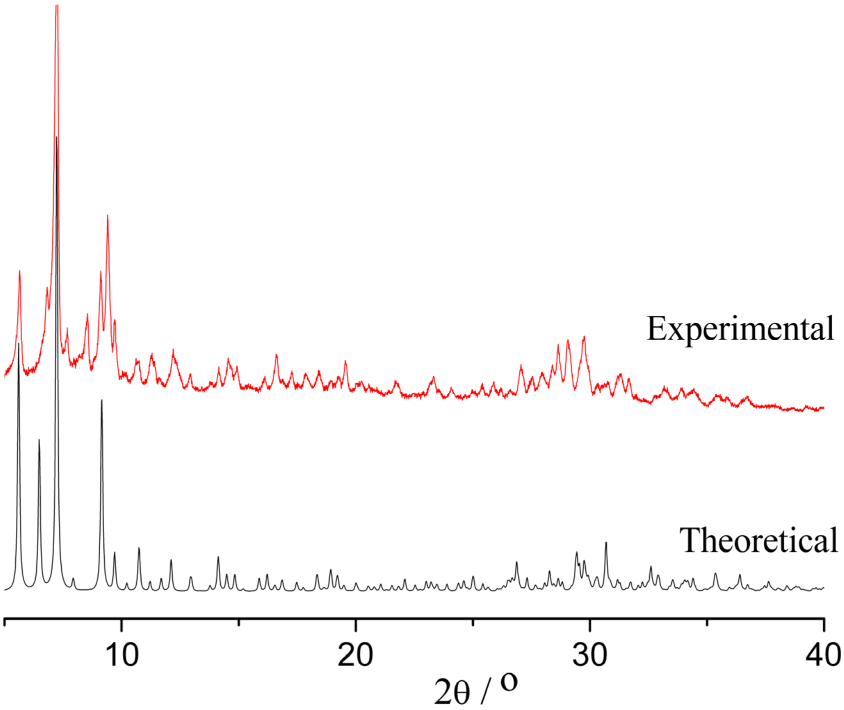

Figure S20. PXRD pattern of bulk **Zn$_4$ (6c)** vs. calculated pattern. Intensity differences may be due to preferred orientation of the powder sample.

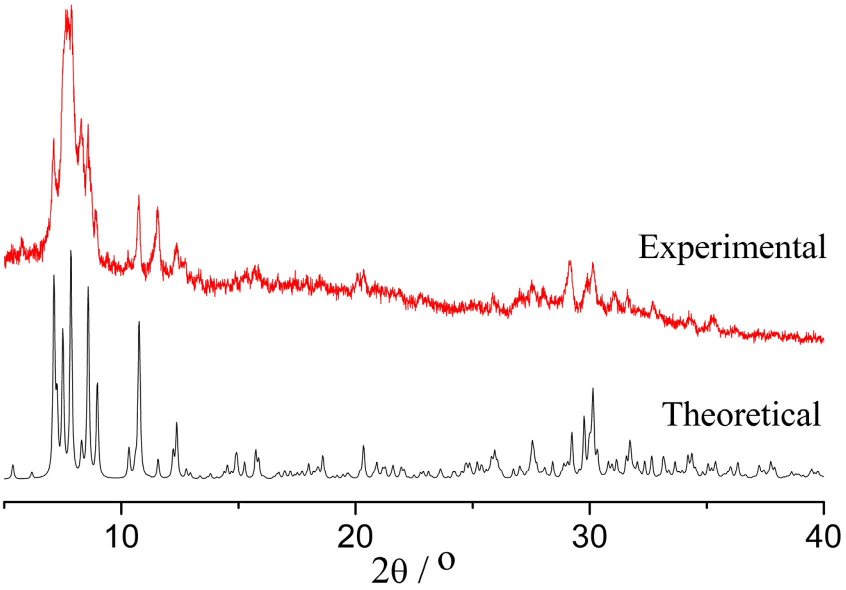

Figure S21. PXRD pattern of bulk **Zn$_{3.5}$ (7)** vs. calculated pattern. Intensity differences may be due to preferred orientation of the powder sample.

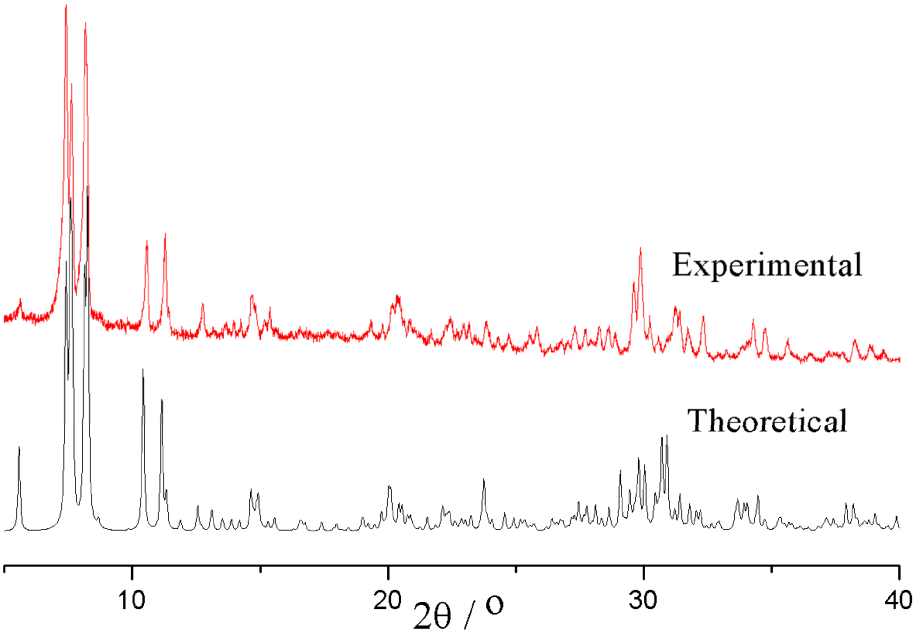

Figure S22. PXRD pattern of bulk **Zn$_3$ (8)** vs. calculated pattern. Intensity differences may be due to preferred orientation of the powder sample.

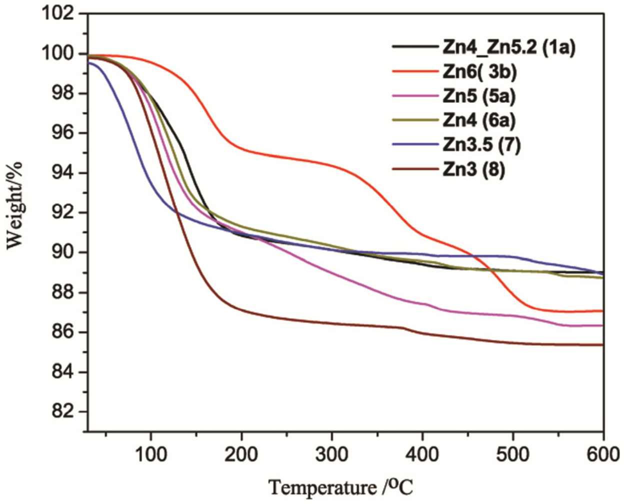

Figure S23. Thermogravimetric curves of **Zn_4_$Zn_{5.2}$ (1a), Zn_6 (3b), Zn_5 (5a), Zn_4 (6a), $Zn_{3.5}$ (7)**, and **Zn_3 (8)**.

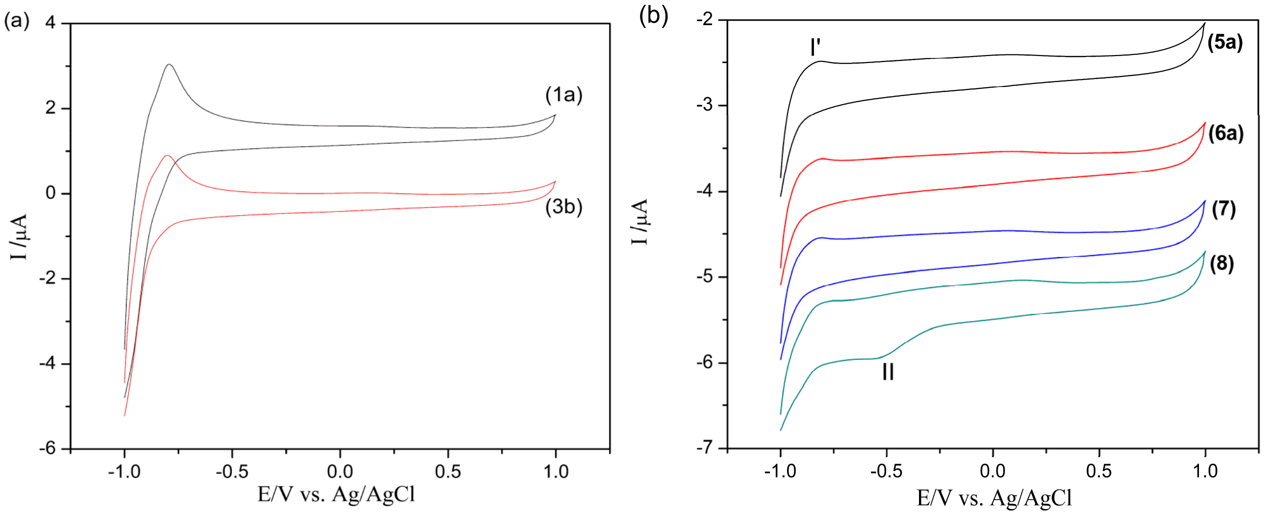

Figure S24. Cyclic voltammograms of (a) **Zn_4_$Zn_{5.2}$ (1a)**, **Zn_6 (3b)** in (1.0 M) NaCl buffer solution, (b) 1 mM **Zn_5 (5a)**, **Zn_4 (6a)**, **$Zn_{3.5}$ (7)**, and **Zn_3 (8)** in (1.0 M) NaCl buffer solution (scan rate 25 mV/s, GCE working electrode, Ag/AgCl reference electrode).

The redox behavior of all compounds was characterized by cyclic voltammetry (CV) in 1.0 M NaCl solution over the potential range of +1.0 to -1.0V (Figure S24). The irreversible redox couple (I-I') between -0.75 and -0.85 V corresponds to the redox processes of the W^{6+} centers. However, the reduction waves (I) of the W centers gradually disappeared with the decrease of the oxidation peak around -0.80 V from Zn_6-containing POMs with hexagonal Zn-centers to the Zn_3-containing POM with trigonal motifs. Moreover, the second reduction peak at -0.544 V (II) was only observed in the compound **Zn_3 (8)**.

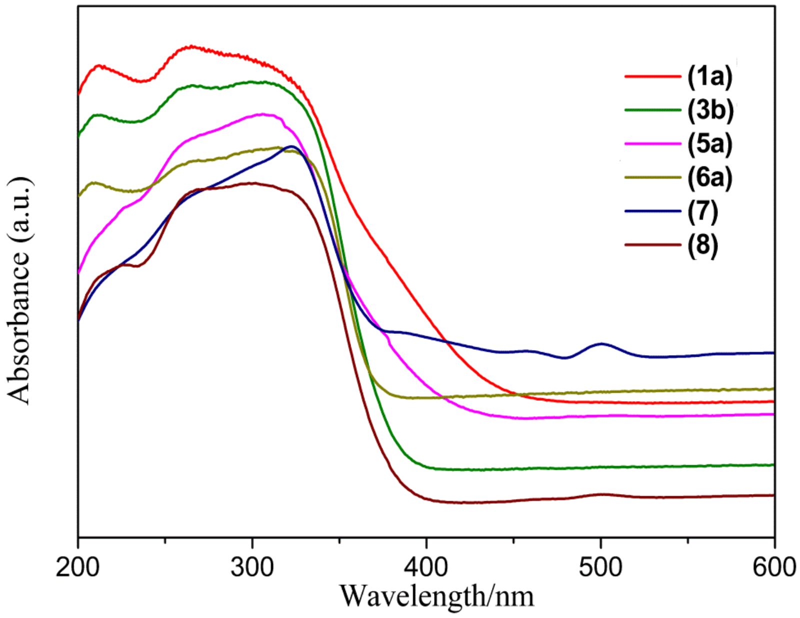

Figure S25. Solid state UV/vis spectra of **Zn_4_$Zn_{5.2}$ (1a)**, **Zn_6 (3b)**, **Zn_5 (4)**, **Zn_5 (5a)**, **Zn_4 (6a)**, **$Zn_{3.5}$ (7)**, and **Zn_3 (8)**.

Solid state UV/Vis spectra of all compounds have two characteristic absorption bands at 200-210 and 260-300 nm in common, with the high energy band corresponding to pπ-dπ charge-transfer transitions of the O_t-W bonds, whereas the low-energy absorption band is due to the pπ-dπ charge-transfer transitions of the $O_{b,c}$-W bonds (Figure S19). FT-IR and Raman spectra of all compounds in the solid state are closely related, and the characteristic peaks are assigned to W-O vibrations from the $[SbW_9O_{33}]^{9-}$ framework (Figures S20, S24, and detailed assignment in Table S7).

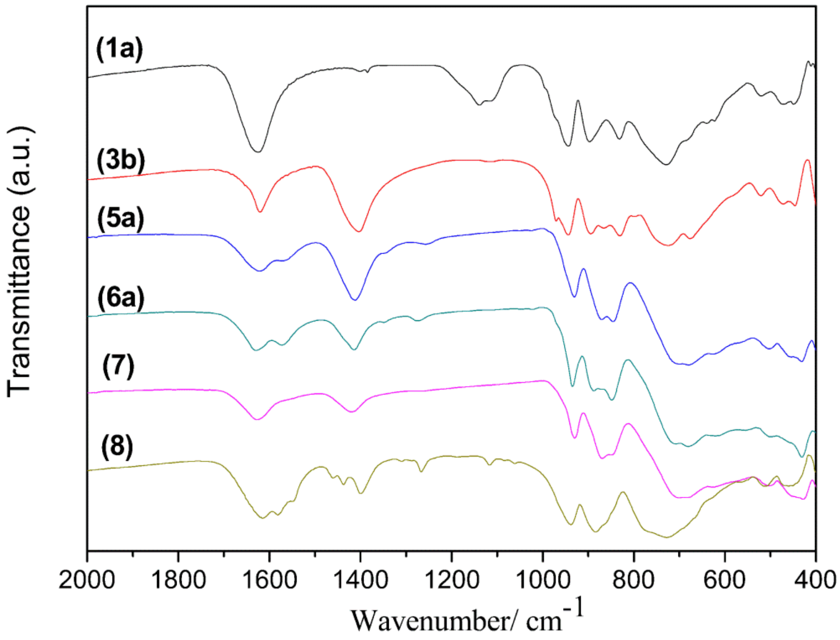

Figure S26. FT-IR spectra of the compounds **Zn$_4$_Zn$_{5.2}$ (1a)**, **Zn$_6$ (3b)**, **Zn$_5$ (5a)**, **Zn$_4$ (6a)**, **Zn$_{3.5}$ (7)**, and **Zn$_3$ (8)** in the solid state.

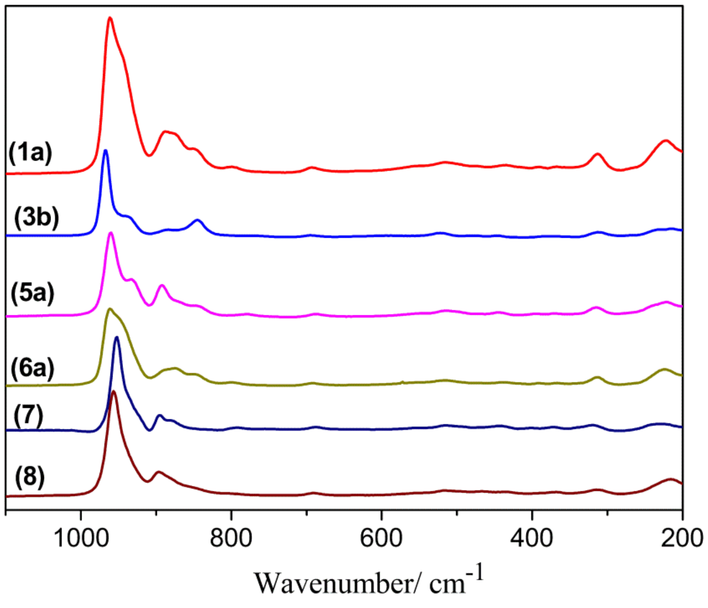

Figure S27. Raman spectra of **Zn$_4$_Zn$_{5.2}$ (1a), Zn$_6$ (3b), Zn$_5$ (5a), Zn$_4$ (6a), Zn$_{3.5}$ (7)**, and **Zn$_3$ (8)** in the solid state.

Table S7. Vibrational features (IR and Raman) for **Zn$_4$_Zn$_{5.2}$ (1a)**, **Zn$_6$ (3b)**, **Zn$_5$ (5a)**, **Zn$_4$ (6a)**, **Zn$_{3.5}$ (7)**, **Zn$_3$ (8)**, and the Na$_9$[B-α-SbW$_9$O$_{33}$]·19.5H$_2$O **{SbW$_9$}** precursor.

Label		**Band assignments^{a} (cm^{-1})**					
{SbW$_9$}		$\delta(HOH)$	$\delta(NH_4)$	$\nu(W{=}O_d)$	$\nu_{as}(W\text{-}O_b)$	$\nu_{as}(W\text{-}O_c)$	$\delta(W\text{-}O_{b,c}\text{-}W)$
	IR	*1617*		*959, 922*	*893*	*770, 710*	
	Raman			*961, 943*	*905, 873*	*795, 688*	*438, 338*
(1a)		$\delta(HOH)$	$\delta(NH_4)$	$\nu(W{=}O_d)$	$\nu_{as}(W\text{-}O_b)$	$\nu_{as}(W\text{-}O_c)$	$\delta(W\text{-}O_{b,c}\text{-}W)$
	IR	*1624*		*946*	*897, 834*	*728*	
	Raman			*961*	*888, 848*	*797,695*	*515*
(3b)		$\delta(HOH)$	$\delta(NH_4)$	$\nu(W{=}O_d)$	$\nu_{as}(W\text{-}O_b)$	$\nu_{as}(W\text{-}O_c)$	$\delta(W\text{-}O_{b,c}\text{-}W)$
	IR	*1624*	*1418*	*946*	*858,824*	*708,665*	*512,434*
	Raman			*996,969*	*886,843*	*693*	*522*
(5a)		$\delta(HOH)$	$\delta(NH_4)$	$\nu(W{=}O_d)$	$\nu_{as}(W\text{-}O_b)$	$\nu_{as}(W\text{-}O_c)$	$\delta(W\text{-}O_{b,c}\text{-}W)$
	IR	*1622*	*1411*	*929*	*870,846*	*698*	*503,430*
	Raman			*960,932*	*892, 843*	*783, 688*	*514, 444*
(6a)		$\delta(HOH)$	$\delta(NH_4)$	$\nu(W{=}O_d)$	$\nu_{as}(W\text{-}O_b)$	$\nu_{as}(W\text{-}O_c)$	$\delta(W\text{-}O_{b,c}\text{-}W)$
	IR	*1628*	*1413*	*937*	*888,848*	*712,679*	*503.430*
	Raman			*959*	*875, 848,*	*799,690*	*517*
(7)		$\delta(HOH)$	$\delta(NH_4)$	$\nu(W{=}O_d)$	$\nu_{as}(W\text{-}O_b)$	$\nu_{as}(W\text{-}O_c)$	$\delta(W\text{-}O_{b,c}\text{-}W)$
	IR	*1626*	*1404*	*935*	*876,837*	*716,673*	*509, 431*
	Raman			*966*	*890, 878,*	*791,697*	*529, 324*
(8)		$\delta(HOH)$	$\delta(NH_4)$	$\nu(W{=}O_d)$	$\nu_{as}(W\text{-}O_b)$	$\nu_{as}(W\text{-}O_c)$	$\delta(W\text{-}O_{b,c}\text{-}W)$
	IR	*1610*		*940, 941*	*883*	*730*	*507,461*
	Raman			*954*	*892, 860,*	*690*	*517, 365*

[a]. $W{=}O_d$, terminal; $W\text{-}O_b$, corner-sharing; $W\text{-}O_c$, edge-sharing.

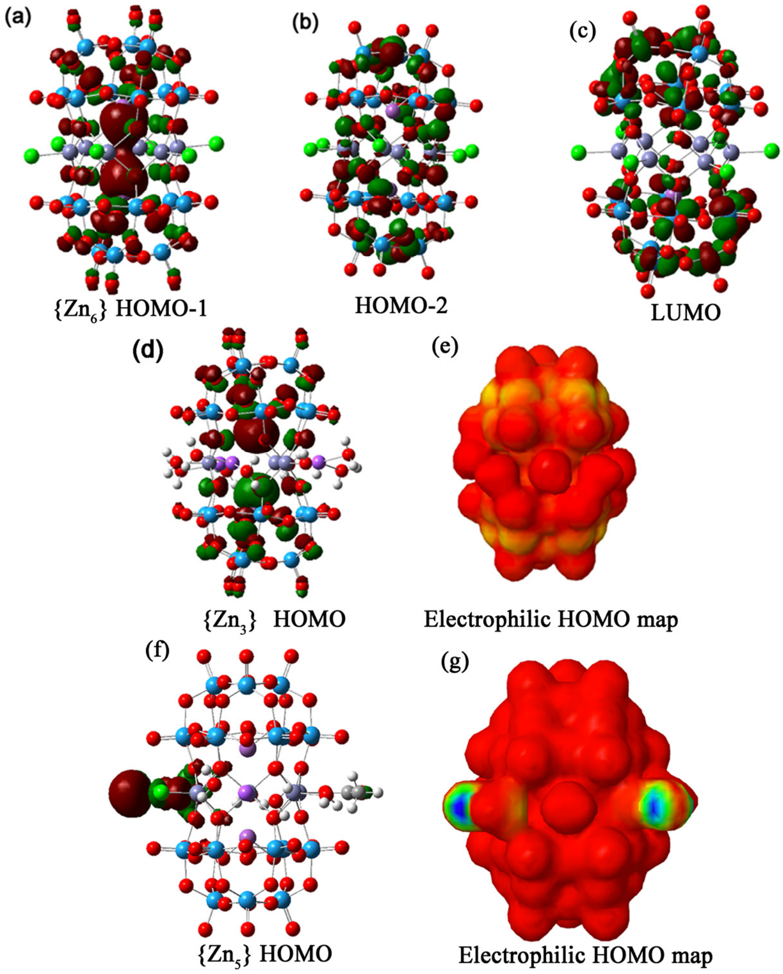

Figure S28. BP86/Def-TZVPP optimized structures of **Zn_6 (3b)**, **Zn_3 (8)**, and **Zn_5 (5a).**

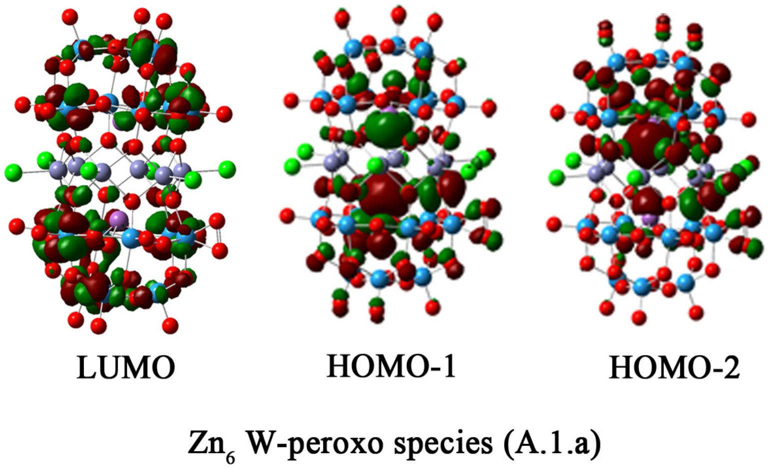

Figure S29. BP86/Def-TZVPP optimized structure of W-peroxo **{Zn_6}** species (**A.1.a)**

Table S8. Oxidation of cyclohexanol with different Zn-POMs and reference POM catalysts.[a]

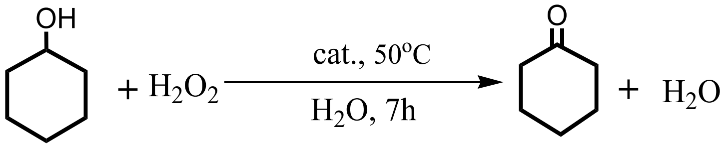

Exp.	**Catalyst**	***T*** **(°C)**	**Yield (%)**[b]
1	$\{Zn_4\_Zn_{5.2}\}$ **(1a)**	50	29
2	Zn_6 **(3b)**	50	31
3	Zn_5 **(5a)**	50	27
4	Zn_4 **(6a)**	50	26
5	Zn_3 **(8)**	50	27
6	Zn_2W_2 **(9)**	50	25
7	$[Sb_2W_{22}O_{74}(OH)_2]^{12-}$	50	22
8	$[SbW_9O_{33}]^{9-}$	50	11
9	$[Sb^VW_6O_{24}]^{7-}$	50	7
10	$[H_2W_{12}O_{42}]^{10-}$	50	14
11	$[P_2W_{18}O_{62}]^{6-}$	50	< 5

[a] Reaction conditions: 0.25 mmol substrate, 1.25 mmol (30 %) H_2O_2, 1.0 μmol catalyst, 1.0 mL H_2O, 50 °C, 7 h. [b] Organic products were identified and quantified by GC-MS and GC with calibrations using pure corresponding standards and dodecane as an internal standard; yield (%) = [cyclohexanone] / initial [cyclohexanol] × 100%. Product distributions were not significantly affected by carrying out the reactions in N_2 atmosphere.

Krebs-type heteropolyanions $[Zn_2Sb_2W_{20}O_{70}]^{10-}$ **$\{Zn_2W_2\}$(9)** (Figure S12e) and tungstoantimonate $[Sb_2W_{22}O_{74}(OH)_2]^{12-}$ (Figure S12d)[S27] also displayed high catalytic activities at 85 °C with respective cyclohexanone yields around 96 % and 92 % (Table 1, entries 7, 8).

Reference POMs with lower nuclearity, such as the trilacunary Keggin POM ligand $Na_9[SbW_9O_{33}]\cdot 19.5H_2O$, the high valent *Anderson*-type Sb-POM $K_5Na_2[Sb^VW_6O_{24}]\cdot 12H_2O$ (Figure S12f), and the paratungstate anion $[H_2W_{12}O_{42}]^{10-}$ (Figure S12g)[S28] were less active with cyclohexanone yields of ca. 77 %, 60 % and 73 %, respectively, at 85 °C (Table 1, entries 9-11), and very low yields of ca. 11 %, 7 % and 14 %, respectively, at 50 °C (Table S8, entries 8-10). Surprisingly, however, the Wells-Dawson-type POM $[P_2W_{18}O_{62}]^{6-}$ (Figure S12h) [S29] with the same W nuclearity as present in the sandwich-type Zn-POM catalyst series exhibited very low catalytic efficiency (21 % at 85°C, Table 1, entry 12) and almost no activity at 50 °C (< 5%, Table S8, entry 11).

Table S9. Cyclohexanol oxidation with **Zn_6 (3b)**.[a]

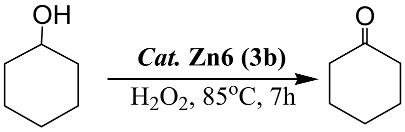

Cycle	Product (Yield %)[c]
	3b[a]
1	cyclohexanone (99)
2	cyclohexanone (98)
3	cyclohexanone (94)

[a] Standard reaction conditions: 0.25 mmol substrate, 1.25 mmol (30 %) H_2O_2, 1.0 μmol catalyst **Zn_6 (3b)**, 1.0 mL H_2O, 85 °C, 7 h. Yields (%) were determined by GC analyses by using pure corresponding samples as calibration standards and dodecane as an internal standard

Table S10. Residual hydrogen peroxide after oxidation of cyclohexanol.[a]

Entry	System	*T* (°C)	Residual H_2O_2 (mmol %)[b]
1	No catalyst	85	36
2	No catalyst	50	90
3	**Zn_6 (3b)**	85	trace
4	**Zn_6 (3b)**	50	27
5	**Cu_3**	85	trace
6	**Cu_3**	50	8

[a] Reaction conditions: 0.25 mmol substrate, 1.25 mmol (30 %) H_2O_2, 1.0 μmol catalyst, 0.50 mL H_2O, 85 or 50 °C, 7 h. [b] Residual Hydrogen peroxide (mmol %) = mmoles of unreacted hydrogen peroxide/initial mmoles of hydrogen peroxide × 100. H_2O_2 contents were quantified by UV/Vis spectroscopy of the characteristic yellow-orange peroxotitanium complex $[Ti(O_2)(OH)(H_2O)_3]^+$.

Further reference experiments with hexa- and tri-copper substituted sandwich-type polyoxometalates $[Cu_6Cl_6(SbW_9O_{33})_2]^{7-}$ **Cu_6** (Figure S12c) and $[Cu_3(SbW_9O_{33})_2]^{12-}$ **Cu3** (Figure S12b) containing a redox-active core proceeded less efficiently at 85 °C than at 50 °C in the presence of **Cu_6** with a hexagonal metal core or **Cu_3** with trigonal copper core motifs (Table 1, entries 13-14; Table S8, entries 12-13). Both Cu-containing sandwich-type POMs **Cu_6** and **Cu_3** were ineffective catalysts affording very low yields (ca. 13% and 10%, respectively, at 85 °C) compared to the Zn/Sb-POM series (yields of 94 - 99 %). Hydrogen peroxide dismutation is generally a competitive process in H_2O_2-assisted oxidation of organic substrates with transition metal catalysts, which frequently proceeds through a radical reaction in the presence of mixed valent transition metal centers (e.g. Fe, Mn, Cu). Hydrogen peroxide utilization efficiency during cyclohexanol oxidation with **Zn_6 (3b)** and **Cu_3** catalysts is compared in Table S10. While hydrogen peroxide dismutation at 50 °C proceeds slowly in the absence of POM catalysts (10 % conversion, cf. Table S10, entry 2), the decomposition rate was quickly increased at elevated temperatures with only 36 % H_2O_2 left at 85 °C (Table S10, entry 1). In the presence of **Zn_6 (3b)** and **Cu_3**, the remaining hydrogen peroxide at 50 °C sharply decreased from ca. 90% (no catalyst) to 27% and 8%, respectively (Table S10, entry 4 and 6), and H_2O_2 was almost quantitatively decomposed at 85 °C (Table S10, entry 3 and 5). **Zn_6(3b)** exclusively catalyzes alcohol oxidation through consumption of residual H_2O_2 at 85 °C, because the redox-inactive Zn^{2+} centers do not catalyze H_2O_2 dismutation. However, this side reaction becomes dominant for Cu-containing POMs so that **Cu_3** is virtually inactive at 85 °C. This outlines the crucial role of the metal core composition in H_2O_2-assisted alcohol oxidation.

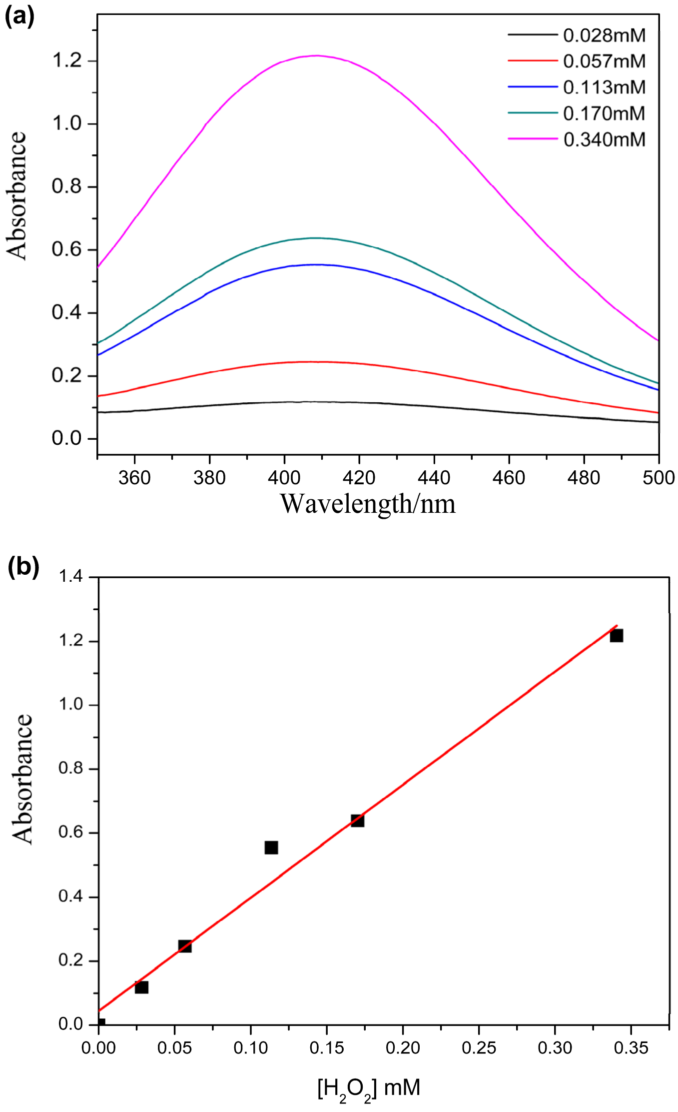

Figure S30. (a) UV/Vis spectra of $Ti(O_2)^{2+}$ complex solutions, [$TiOSO_4$] = 24.39 mM in 2.15 mM H_2SO_4, [H_2O_2] = 0.028-0.340 mM; (b) absorbance values at 410 nm *vs.* [H_2O_2].

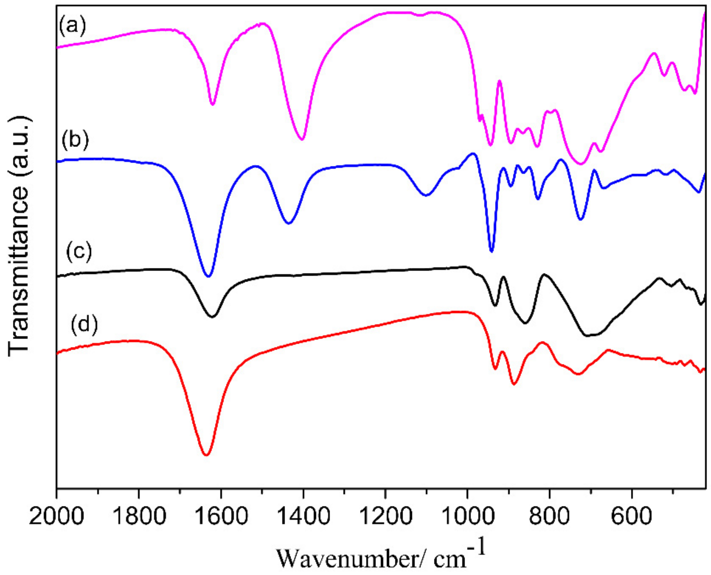

Figure S31. FT-IR spectra of (a) **Zn$_6$ (3b)** in the solid state, (b) **Zn$_6$ (3b)** in aqueous solution, (c) **{Cu$_3$}** in the solid state and (d) **{Cu$_3$}** in aqueous solution.

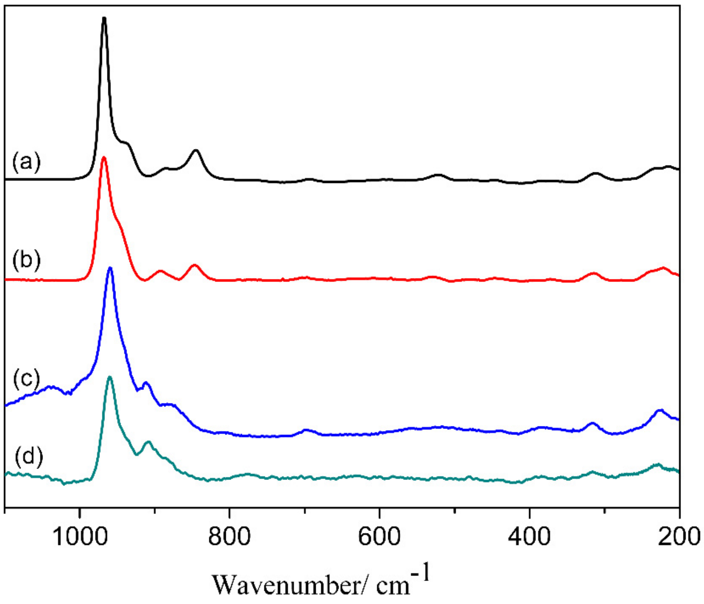

Figure S32. Raman spectra of (a) **Zn$_6$ (3b)** in the solid state, (b) **Zn$_6$ (3b)** in aqueous solution, (c) **{Cu$_3$}** in the solid state and (d) **{Cu$_3$}** in aqueous solution.

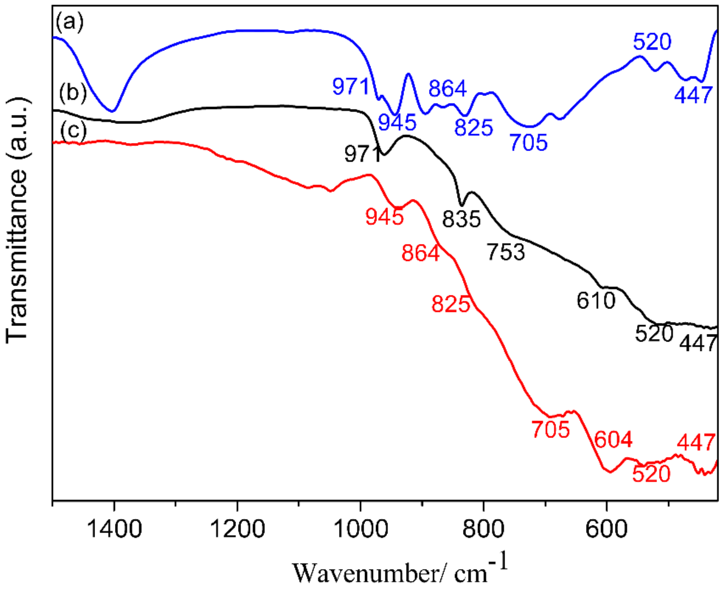

Figure S33. FT-IR spectra of (a) **Zn₆ (3b)** in the solid state, (b) **Zn₆ (3b)** after treatment with a 50-fold excess of excess of H_2O_2 in aqueous solution, (c) after removal of excess 30% H_2O_2 with aqueous KI solution.

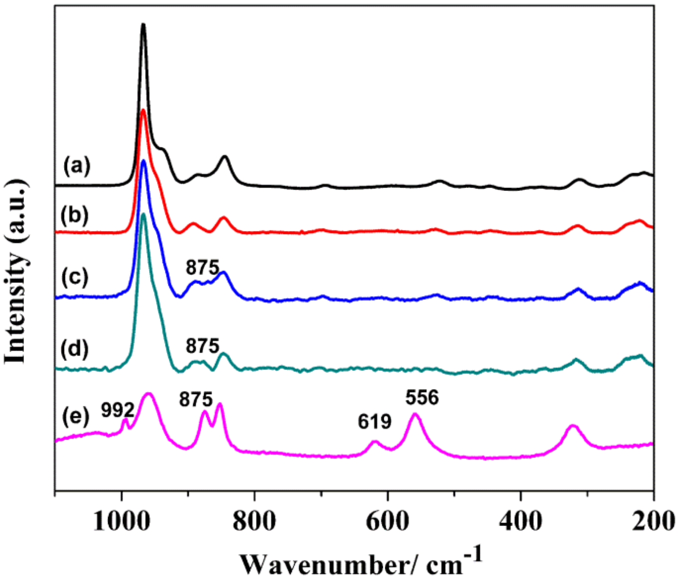

Figure S34. Raman spectra of **Zn6 (3b)**: (a) solid state; (b) in the absence of H_2O_2 in aqueous solution; (c) $[H_2O_2]$/[**(3b)**] = 1:1 in aqueous solution; (d) $[H_2O_2]$/[**(3b)**] = 5:1 in aqueous solution; (e) $[H_2O_2]$/[**(3b)**] = 50:1 in aqueous solution.

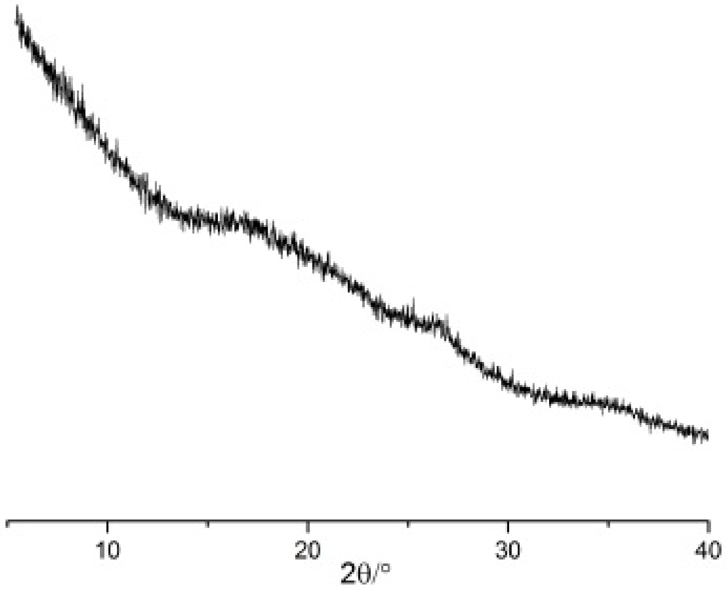

Figure S35. PXRD pattern of the insoluble precipitation after catalysis.

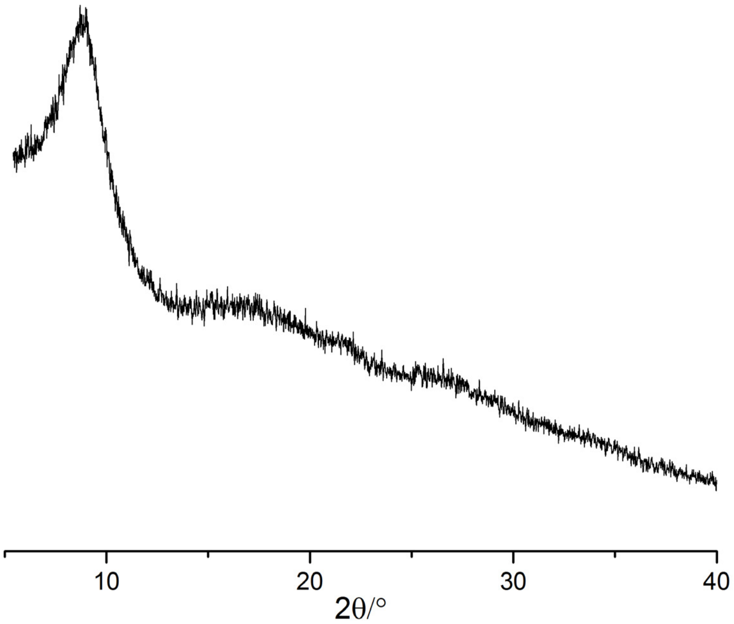

Figure S36. PXRD pattern of the true catalyst after catalysis.

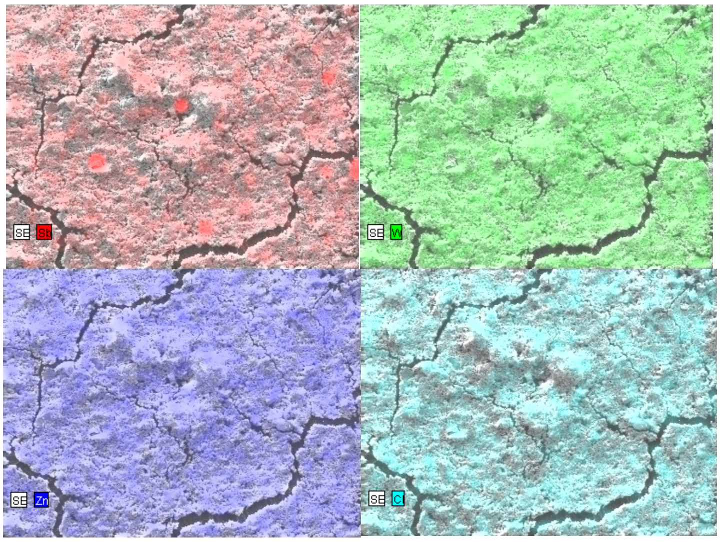

Figure S37. EDX mapping of the true catalyst after catalysis.

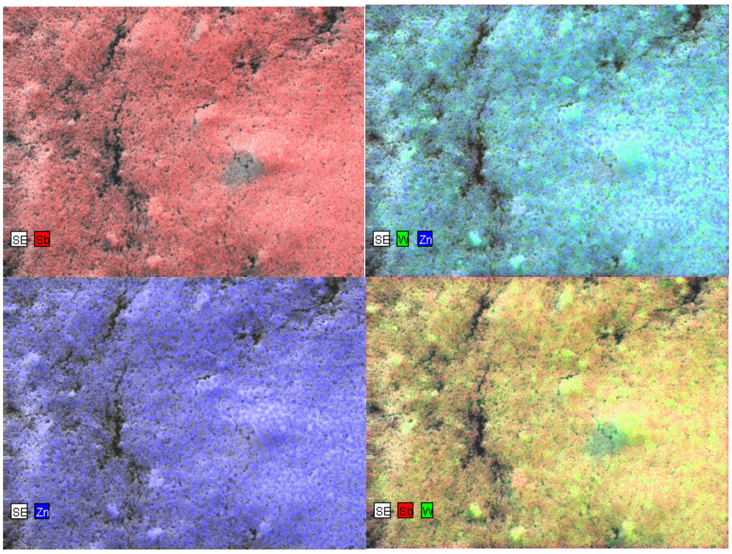

Figure S38. EDX mapping of the insoluble precipitate after catalysis.

Table S11. Vibrational features (FT-IR) for true catalyst and possible matching POMs

List of Zn-POMs	**Zn/W atomic ratio**	**FT-IR**	**Ref.**
True catalyst	1:3.4	937, 866, 737, 615, 534, 438 cm^{-1}	
$Na_{12}(WZn_3(H_2O)_2(ZnW_9O_{34})_2)$	1:3.8	722, 765, 873, 923 cm^{-1}	[S30]
$[Zn_6(imi)_6(H_3AsW_9O_{33})_2]$	1:3	840, 953, 696, 526 cm^{-1}	[S31]
$Na_{12}(Zn_4(H_2O)_2(GeW_9O_{34})_2)$	1:4.5	946, 888, 837, 772, 705, 511, 454 cm^{-1}	[S32]
$Na_{10}[Sb_2W_{18}Zn_3O_{66}(H_2O)_3]$	1:6	963, 942, 895, 881, 854, 780, 736, 507, 461, 437 cm^{-1}	[S33]
$(Me_4N)_6[ZnW_{12}O_{40}]$	1:4	943, 881, 785, 530, 442, 400 cm^{-1}	[S34]

Table S12. ICP-MS measurements of the **Zn_6 (3b)** pristine and true catalyst

Zn_6 (3b) pristine	Zn:W	1:3.06
	Sb:Zn	1:2.93
True catalyst	Zn:W	1:3.37
	Sb:Zn	1:22.74

Table S13. EDX element ratios of the insoluble precipitate formed from **Zn_6 (3b)** immediately after the onset of catalysis.

Element	**Precipitate of Zn_6 (3b) [at.%]**	**Error [wt.%]**
Zn K-series	28.08	0.7
Sb L-series	68.13	1.8
W L-series	3.79	0.5

Table S14. EDX analyses of element ratios of post-catalytic **Zn$_5$ (5b)** and **Zn$_4$ (6a)** isolated from the aqueous phase and of their respective precipitations formed at the onset of catalysis.

Element	**Zn$_5$ (5b)** post-cat. [at. %]	**Zn$_4$ (6a)** post-cat. [at. %]
Zn K-series	15.00	14.00
Sb L-series	4.99	4.46
W L-series	80.01	81.54

Element	**Zn$_5$ (5b)** precipitation [at. %]	**Zn$_4$ (6a)** precipitation [at. %]
Zn K-series	8.09	7.42
Sb L-series	70.26	71.68
W L-series	21.66	20.90

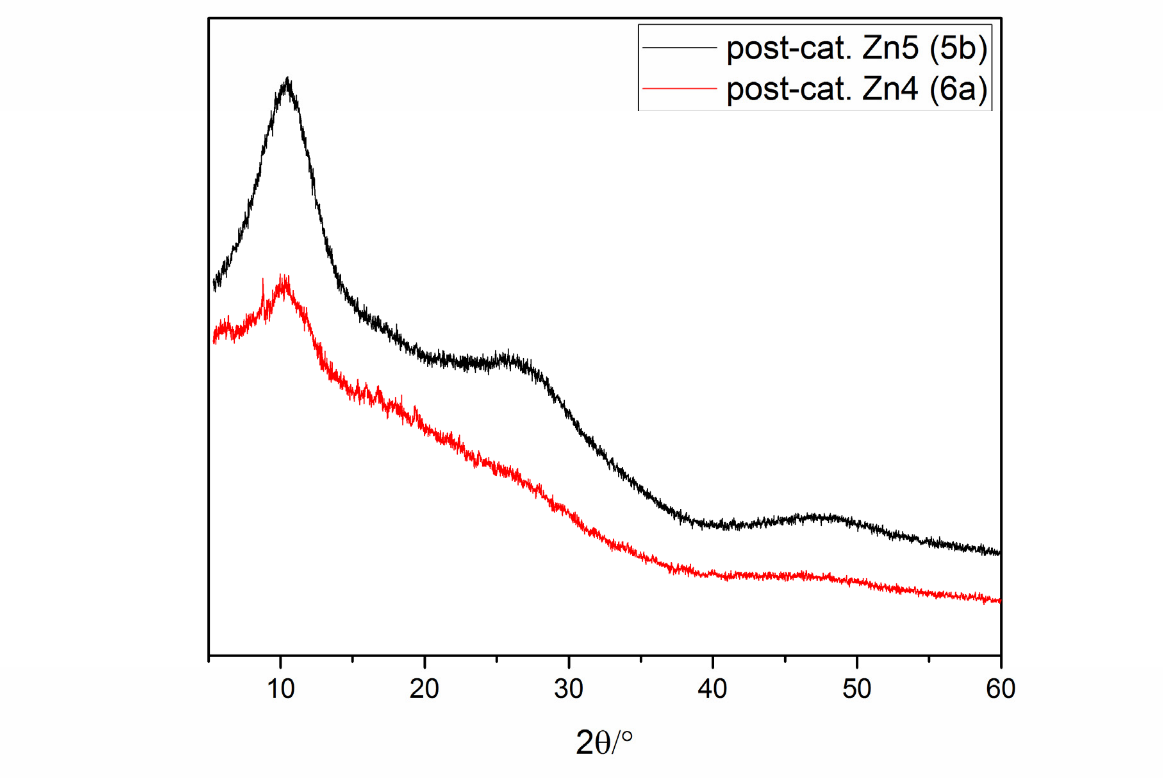

Figure S39. PXRD patterns of **Zn$_5$ (5b)** and **Zn$_4$ (6a)** after 1st cyclohexanol oxidation.

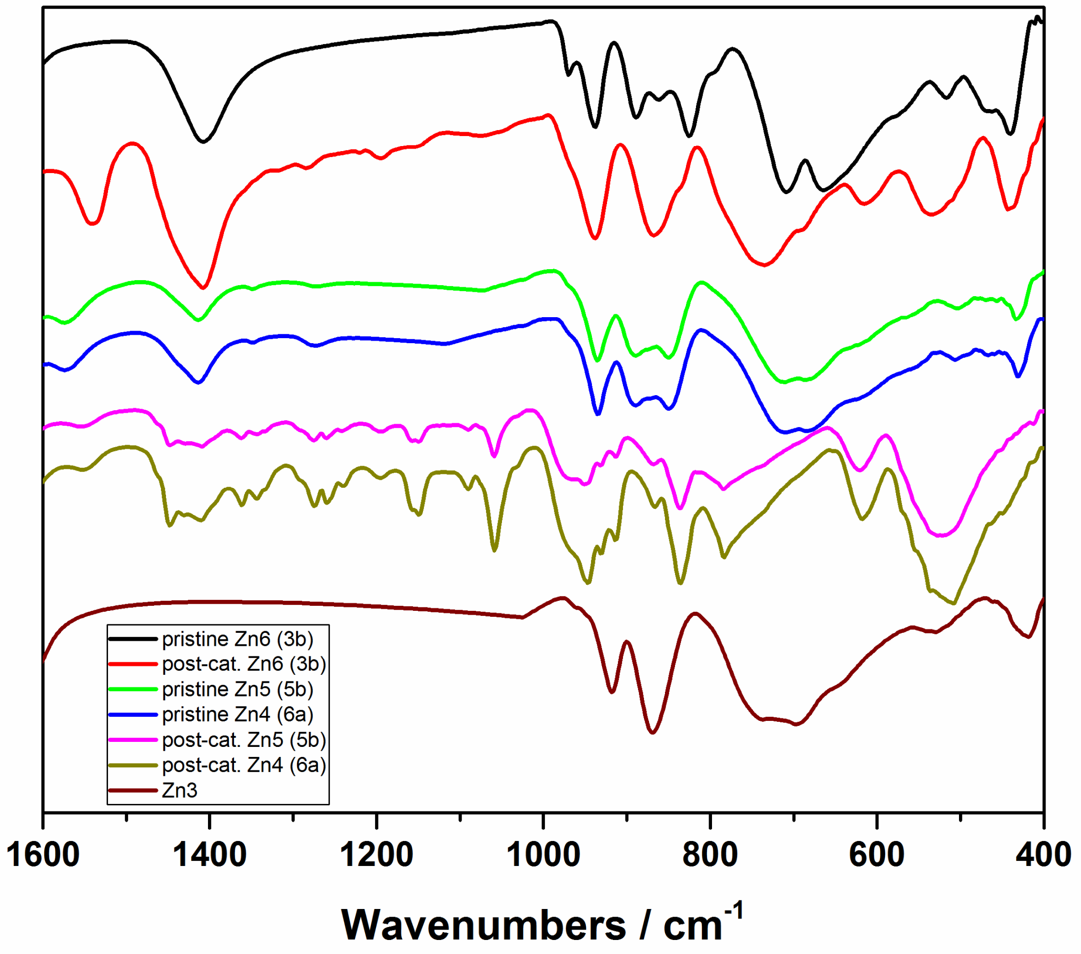

Figure S40. FT-IR spectra of **Zn_6(3b)** in the solid state, **Zn_6(3b)** after 1st cyclohexanol oxidation, pristine **Zn_5 (5b)** and **Zn_4 (6a)**, compared to **Zn_5 (5b)** and **Zn_4 (6a)** after 1st cyclohexanol oxidation and $[WZn_3(H_2O)_2(ZnW_9O_{34})_2]^{12-}$ as reference in the solid state.

Table S15. Main interatomic distances, atomic coordination numbers (*N*), and Debye-Waller factors (σ^2) calculated from nonlinear least-squares fitting of the experimental W-L_3-edge FT|$k^3\chi(k)$| spectra for pristine $[Zn_6Cl_6(SbW_9O_{33})_2]^{12-}$, $Na_2WO_4{\cdot}2H_2O$, $[WZn_3(H_2O)_2(ZnW_9O_{34})_2]^{12-}$, $[SbW_9O_{33}]^{9-}$ and RMC-EXAFS fitting of the experimental W-L_3-edge FT|$k^3\chi(k)$| spectra of the true catalyst.

$Na_2WO_4{\bullet}2H_2O$ [S_0^2≈0.91, ΔE_0≈5.6 eV]			$[SbW_9O_{33}]^{9-}$ [S_0^2≈0.99, ΔE_0≈6.9 eV]			$[WZn_3(H_2O)_2(ZnW_9O_{34})_2]^{12-}$ [S_0^2≈1.05, ΔE_0≈2.1 eV]			Pre $[Zn_6Cl_6(SbW_9O_{33})_2]^{12-}$ [S_0^2≈0.99, ΔE_0≈1.83 eV]			True catalyst RMC-EXAFS	
W-O (±0.008 Å)	$N_{W\text{-}O}$	$\sigma^2_{W\text{-}O}$	W-O (±0.008 Å)	$N_{W\text{-}O}$	$\sigma^2_{W\text{-}O}$	W-O (±0.008 Å)	$N_{W\text{-}O}$	$\sigma^2_{W\text{-}O}$	W-O (±0.008 Å)	$N_{W\text{-}O}$	$\sigma^2_{W\text{-}O}$	W-O (±0.008 Å)	$N_{W\text{-}O}$
1.786	4	0.0005	1.702	1	0.0011	1.759	1	0.0083	1.709	1	0.0103	1.634-1.692	1
W-Na (±0.008 Å)	$N_{W\text{-}Na}$	$\sigma^2_{W\text{-}Na}$	1.867	2	0.0045	1.849	2	0.0023	1.843	1	0.0112	1.818-1.846	1
3.665	2	0.0017	1.958	2	0.0078	1.934	2	0.0032	1.859	1	0.0098	1.872-1.894	1
3.691	1	0.0015	2.598	1	0.0026	2.145	1	0.0008	1.971	2	0.0095	1.971-2.020	1
3.738	1	0.0021	W-W (±0.008 Å)	$N_{W\text{-}W}$	$\sigma^2_{W\text{-}W}$	W-W (±0.008 Å)	$N_{W\text{-}W}$	$\sigma^2_{W\text{-}W}$	2.263	1	0.0101	2.041-2.092	1
3.762	2	0.0020	3.549	2	0.0013	3.253	1	0.0084	W-W (±0.008 Å)	$N_{W\text{-}W}$	$\sigma^2_{W\text{-}W}$	2.224-2.256	1
			3.695	2	0.048	3.325	1	0.0014	3.355	2	0.0033	W-W (±0.008 Å)	$N_{W\text{-}W}$
									3.665	2	0.0030	3.163-3.196	1
												3.437-3.472	1
												3.560-3.651	1
												3.708-3.849	1

Table S16. Main interatomic distances, atomic coordination numbers (*N*), and Debye-Waller factors (σ^2) calculated from nonlinear least-squares fitting of the experimental Zn-*K*-edge EXAFS spectra FT|$k^3\chi(k)$| of pristine $[Zn_6Cl_6(SbW_9O_{33})_2]^{12-}$, $[WZn_3(H_2O)_2(ZnW_9O_{34})_2]^{12-}$ and RMC-EXAFS fitting of the experimental Zn-*K*-edge FT|$k^3\chi(k)$| spectra of the true catalyst.

$[WZn_3(H_2O)_2(ZnW_9O_{34})_2]^{12-}$ [S_0^2≈0.98, ΔE_0≈1.831 eV]			Pre $[Zn_6Cl_6(SbW_9O_{33})_2]^{12-}$ [S_0^2≈0.98, ΔE_0≈1.831 eV]			True catalyst RMC-EXAFS	
Zn-O (±0.008 Å)	$N_{Zn\text{-}O}$	$\sigma^2_{Zn\text{-}O}$	Zn-O (±0.008 Å)	$N_{Zn\text{-}O}$	$\sigma^2_{Zn\text{-}O}$	Zn-O (±0.008 Å)	$N_{Zn\text{-}O}$
1.859	1	0.0042	2.084	4	0.0094	1.946-2.042	2
1.948	1	0.0053	Zn-Cl (±0.008 Å)	$N_{Zn\text{-}Cl}$	$\sigma^2_{Zn\text{-}Cl}$	2.072-2.086	2
2.054	2	0.0067	2.240	1	0.0051	2.119-2128	2
2.086	2	0.0038	Zn-Zn (±0.008 Å)	$N_{Zn\text{-}Zn}$	$\sigma^2_{Zn\text{-}Zn}$	Zn-Zn (±0.008 Å)	$N_{Zn\text{-}Zn}$
Zn-Zn (±0.008 Å)	$N_{Zn\text{-}Zn}$	$\sigma^2_{Zn\text{-}Zn}$	3.203	2	0.0098	3.212-3.435	1
3.209	3	0.0035	Zn-W (±0.008 Å)	$N_{Zn\text{-}W}$	$\sigma^2_{Zn\text{-}W}$	5.321-5.394	1
3.338	2	0.0038	3.489	2	0.0076	Zn-W (±0.008 Å)	$N_{Zn\text{-}W}$
Zn-W (±0.008 Å)	$N_{Zn\text{-}W}$	$\sigma^2_{Zn\text{-}W}$	3.558	2	0.0060	3.444-3.591	2
3.491	5	0.0056				3.731-3.926	2
3.641	2	0.0068					

References

[S1] Bösing, M.; Loose, I.; Pohlmann, H.; Krebs, B. *Chem. Eur. J.* **1997**, 8, 1232-1237. IR (KBr disk): 925 (m), 891 (s), 769 (s), 708 cm^{-1} (s).

[S2] Ni, L.; Patscheider, J.; Baldridge, K. K.; Patzke, G. R.; *Chem. Eur. J.* **2012**, *18*, 13293-13298.

[S3] Kortz, U.; Al-Kassem, N. K.; Savelieff, M. G.; Al Kadi, N. A.; Sadakane, M. *Inorg. Chem.* **2001**, *40*, 4742-4749.

[S4] (a) Loose, I.; Droste, E. B; Sing, M.; Pohlmann, H.; Dickmann, M. H.; Rosu, C.; Pope, M. T.; Krebs, B. *Inorg. Chem.* **1999**, 38, 2688-2694; (b) Piepenbrink, M.; Limanski, E.M.; Krebs, B. *Z. Anorg. Allg. Chem.* **2002**, *628*, 1187-1191.

[S5] Oxford Diffraction, CrysAlis CCD and CrysAlis RED, Oxford Diffraction Ltd., Abingdon, UK, **2005**.

[S6] Farrugia, L. J. *J. Appl. Crystallogr.* **1999**, *32*, 837-838.

[S7] Sheldrick, G. M. SHELX97, *Programs for Crystal Structure Analysis*; Release 97-2; University of Göttingen, Göttingen: Germany, **1997**.

[S8] (a) Sadakane, M.; Dickman, M. H.; Pope, M. T. *Inorg. Chem.* **2001**, *40*, 2751-2755; (b) du Peloux, C.; Dolbecq, A.; Mialane, P.; Marrot, J.; Rivière, E.; Sécheresse, F. *Inorg. Chem.* **2002**, *41*, 7100-7104; (c) Gaunt, A. J.; May, L.; Collison, D.; Fox, D. *Inorg. Chem.* **2003**, *42*, 5049-5051; (d) Lei, C.; Mao, J.-G.; Sun, Y.-Q.; Song, J.-L. *Inorg. Chem.* **2004**, *43*, 1964-1968; (e) Mazeaud, A.; Dromzee, Y.; Thouvenot, R. *Inorg. Chem.* **2000**, *39*, 4735-4740; (f) Juraja, S.; Vu, T.; Richardt, P. J. S.; Bond, A. M.; Cardwell, T. J.; Cashion, J. D.; Fallon, G. D.; Lazarev, G.; Moubaraki, B.; Murray, K. S.; Wedd, A. G. *Inorg. Chem.* **2002**, *41*, 1072-1078; (g) Dolbecq, A.; Cadot, E.; Eisner, D.; Sécheresse, F. *Inorg. Chem.* **1999**, *38,* 4217-4223; (h) Villanneau, R.; Proust, A.; Robert, F.; Viellet, P.; Gouzerh, P. *Inorg. Chem.* **1999**, *38*, 4981-4985; (i) Volkmer, D.; Bredenkötter, B.; Tellenbröker, J.; Kögerler, P.; Kurth, D. G.; Lehmann, P.; Schnablegger, H.; Schwahn, D.; Piepenbrink, M.; Krebs, B. *J. Am. Chem. Soc.* **2002**, *124*, 10489-10496. (j) Ni, L.; Patzke, G. R. *CrystEngComm* **2012**, *14*, 6778-6782.

[S9] Ravel, B. & Newville, M. ATHENA, ARTEMIS, HEPHAESTUS: data analysis for X-ray absorption spectroscopy using IFEFFIT. *J. Synchrotron. Rad.* **2005** *12*, 537-541

[S10] Ankudinov, A. L., Ravel, B., Rehr, J. J. & Conradson, S. D. Real-space multiple-scattering calculation and interpretation of X-ray absorption near-edge structure. *Phys. Rev. B.* **1998,** *58*, 7565–7576

[S11] Schmidt, M.W.; Baldridge, K.K.; Boatz, J.A.; Elbert, S.T.; Gordon, M.S.; Jensen, J.H.; Koseki, S.; Matsunaga, N.; Nguyen, K.A.; Su, S.; Windus, T.L. The General Atomic and Molecular Electronic Structure System. *J. Comp. Chem.* **1993**, *14*, 1347.

[S12] Frisch, M. J.; Trucks, G. W.; Schlegel, H. B.; Scuseria, G. E.; Robb, M. A.; Cheeseman, J. R.; Scalmani, G.; Barone, V.; Mennucci, B.; Petersson, G. A.; Nakatsuji, H.; Caricato, M.; Li, X.; Hratchian,

H. P.; Izmaylov, A. F.; Bloino, J.; Zheng, G.; Sonnenberg, J. L.; Hada, M.; Ehara, M.; Toyota, K.; Fukuda, R.; Hasegawa, J.; Ishida, M.; Nakajima, T.; Honda, Y.; Kitao, O.; Nakai, H.; Vreven, T.; Montgomery, J. A., Jr., Peralta, J. E.; Ogliaro, F.; Bearpark, M.; Heyd, J. J.; Brothers, E.; Kudin, K. N.; Staroverov, V. N.; Keith, T.; Kobayashi, R.; Normand, J.; Raghavachari, K.; Rendell, A.; Burant, J. C.; Iyengar, S. S.; Tomasi, J.; Cossi, M.; Rega, N.; Millam, J. M.; Klene, M.; Knox, J. E.; Cross, J. B.; Bakken, V.; Adamo, C.; Jaramillo, J.; Gomperts, R.; Stratmann, R. E.; Yazyev, O.; Austin, A. J.; Cammi, R.; Pomelli, C.; Ochterski, J. W.; Martin, R. L.; Morokuma, K.; Zakrzewski, V. G.; Voth, G. A.; Salvador, P.; Dannenberg, J. J.; Dapprich, S.; Daniels, A. D.; Farkas, O.; Foresman, J. B.; Ortiz, J. V.; Cioslowski, J.; Fox, D. J. Gaussian 09, Revision E.01, Gaussian, Inc., Wallingford CT, **2013**.

[S13] Becke, A.D. *Phys. Rev. A.*, **1988**, *38*, 3098-100.

[S14] Perdew, J.P. *Phys. Rev. B.*, **1986**, *33*, 8822-24.

[S15] Dunning, T. H., Jr.; Hay, P. J. *Modern Theoretical Chemistry*; Plenum: New York, 1976.

[S16] Weigend, F.; Ahlrichs, R. *Phys. Chem. Chem. Phys*. **2005**, *7,* 3297-3305.

[S17] Hay, P. J.; Wadt, W. R. *J. Chem. Phys.* **1985**, *82*, 299-310.

[S18] Hay, P. J.; Wadt, W. R. *J. Chem. Phys.* **1985**, *82*, 270-283.

[S19] Wadt, W. R.; Hay, P. J. *J. Chem. Phys.* **1985**, *82*, 284-298.

[S20] Klamt, A.; Schüürmann, G. *J. Chem. Soc. Perkin Trans 2*, **1993**, 799.

[S21] Baldridge, K.; Klamt, A. *J. Chem. Phys.* **1997**, *106*, 6622-6633.

[S22] Klamt, A.; Jonas, V.; Bürger, T.; Lohrenz, C. W. *J. Phys. Chem.* **1998**, *102*, 5074-5085.

[S23] Hanwell, M.; Curtis, D.; Lonie, D.; Vandermeersch, T.; Zurek, E.; Hutchison, G. *J. Cheminform.* **2012**, *4*, 173.

[S24] http://www.webmo.net/index.html.

[S25] Tucker, M. G., Keen, D. A., Dove, M. T., Goodwin, A. L. & Hui, Q. RMCProfile: reverse Monte Carlo for polycrystalline materials. *J. Phys.: Condens. Matter.* **2007**, *19*, 1-16

[S26] (a) Krayzman, V., Levin, I., Wocik, J. C., Proffen, T., Vanderah, T. A. & Tucker, M. G. A. *J. Appl. Crystallogr.* **2009**, *42*, 867-877; (b) Németh, K., Chapman, K. W., Balasubramanian, M., Shyam, B. Chupas, P. J. Heald, S. M., Newville, M. Klingler, R. J., Winans, R. E., Almer, J. D. Sandi, G. & Srajer, G. *J. Chem. Phys.* **2012**, *136*, 074105-1-10; (c) Triana, C. A., Araujo, C. M., Ahuja, R., Niklasson, G. A. & Edvinsson, T. *Phys. Rev. B.* **2016**, *94*, 165129-1-9; (d) Triana, C. A., Araujo, C. M., Ahuja, R., Niklasson, G. A. & Edvinsson, T. *Sci. Rep.* **2017**, *7*, 2044.

[S27] Bösing, M., Loose, I., Pohlmann, H. & Krebs, B. *Chem. - Eur. J.***1997**, *3*, 1232–1237.

[S28] Redrup, K. V.; Weller, M. T. *Dalton Trans.* **2009**, 4468–4472.

[S29] (a) Graham, C. R.; Finke, R. G. *Inorg. Chem.* **2008**, *47*, 3679–3686. (b) Randall, W. J.; Droege, M. W.; Mizuno, N.; Nomiya, K.; Weakley, T. J. R.; Finke, R. G.; Isern, N.; Salta, J.; Zubieta, J. In *Inorganic Syntheses*; Darensbourg, M. Y., Ed.; Inorganic Syntheses 32; John Wiley & Sons, Inc: Hoboken, NJ, USA, **1998**; 167–185. (c) Finke, R. G.; Droege, M. W.; Domaille, P. J. *Inorg. Chem.* **1987**, *26*, 3886–3896.

[S30] Morris, A. M.; Anderson, O.P.; Finke, R. G. *Inorg. Chem.* **2009**, *48*, 4411-4420.

[S31] Zhao, Z.; Zhou, B.; Zheng, S.; Su, Z.; Wang, C. *Inorg. Chim. Acta* **2009**, *362*, 5038-5042.

[S32] Kortz, U.; Nellutla, S.; Stowe, A. C.; Dalal, N. S.; Rauwald, U.; Danquah, W.; Ravot, D. *Inorg. Chem.* **2004**, *43*, 2308-2317.

[S33] Kortz, U.; Al-Kassem, N. K.; Savelieff, M. G.; Al Kadi, N. A.; Sadakane, M. *Inorg. Chem*. **2001**, *40*, 4742-4749.

[S34] Nakajima, K.; Eda, K.; Himeno, S. *Inorg. Chem.* **2010**, *49*, 5212-5215.